EFFECTIVE DIELECTRIC RESPONSE IN INHOMOGENEOUS DIELECTRICS

Jan Petzelt, Ivan Rychetský
Institute of Physics, Academy of Science of the Czech Rep.
Na Slovance 2, 182 21 Praha 8, Czech Republic

Outline:

1. Introduction: inhomogeneous media, quasistatic approximation
2. Maxwell – Garnett and Bruggeman model, effective medium approximation (EMA);
3. Upper and lower bound, Hashin – Shtrikman model
4. Brick-wall model, equivalent circuits approach;
5. Bergman approach
6. Generalised brick-wall model
7. AC response, effective dielectric function
8. Examples: $SrTiO_3$ ceramics and films, $PbZrO_3$ ceramics, $BaTiO_3$ ceramics, nano-ceramics and films.

Dielectrically inhomogeneous media - examples:

Composites (0-3 connectivity: dielectric – ferroelectric, dielectric – metal (cermet), ferroelectric – metal, 1-3 connectivity: fiber composites, 2-2 connectivity: lamellar composites, multilayers, heterostructures and superlattices);

Ceramics and thin films (isotropic (cubic) grains – grain boundaries (passive, dead layers with reduced permittivity or boundaries with different conductivity or losses), dielectrically anisotropic grains;

Polydomain ferroelectric and other (twinned) ferroic crystals;

Relaxor ferroelectrics and dipolar glasses (polar nano-clusters embedded into non-polar matrix) - specific feature: clusters are dynamic at higher temperatures and contribute strongly to the dielectric response by their reorientation and/or volume fluctuations (breathing);

Quasistatic (electrostatic) approximation:

Sharp boundaries among the components and homogeneous electric field E within individual components $\Rightarrow$ magnetic field effects in non-magnetic media ($\mu = 1$) can be neglected.

Maxwell – Garnett model:

$x_1 + x_2 = 1$

Relative volume x_2
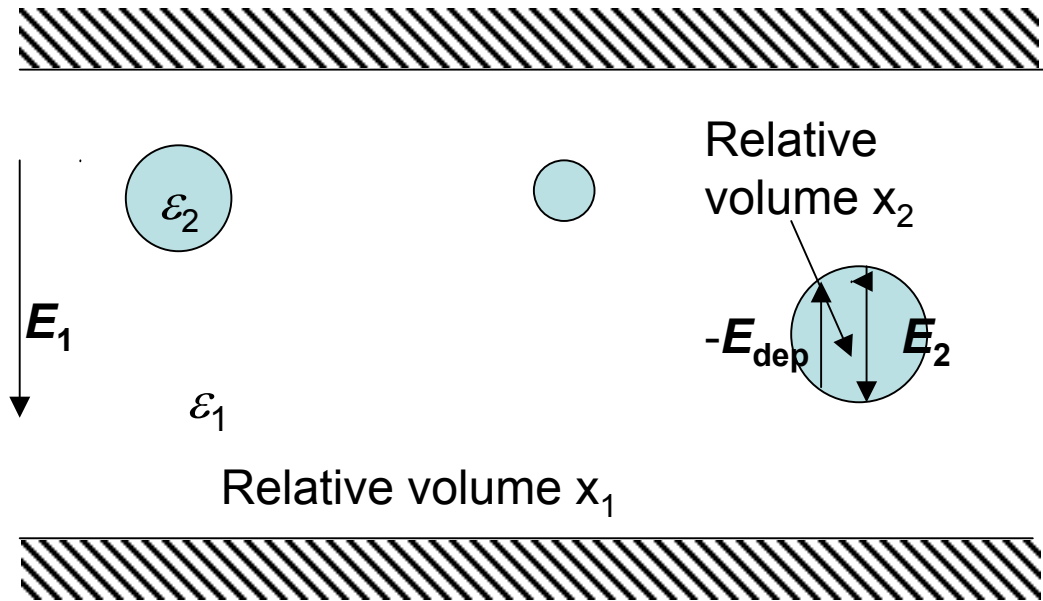
$$E_2 = E_1 + E_{dep} = 3\varepsilon_1/(\varepsilon_2 + 2\,\varepsilon_1) \cdot E_1$$

assuming negligible interaction among embedded particles, i.e. $x_2 \ll x_1$

$-E_{dep} \qquad E_2$

E_1

ε_2

ε_1

Relative volume x_1

E_{dep} is homogeneous in spherical (generally ellipsoidal) particles

Effective dielectric response:

Average macroscopic field: $\qquad \bar{E} = x_1 E_1 + x_2 E_2$

Average dielectric displacement: $\qquad \bar{D} = x_1 \varepsilon_1 E_1 + x_2\, \varepsilon_2 E_2 \equiv \varepsilon_{eff}\, \bar{E}$

$$\varepsilon_{eff} = \frac{\overline{D}}{\overline{\overline{E}}} = \frac{x_1 \varepsilon_1 E_1 + x_2 \varepsilon_2 E_2}{x_1 E_1 + x_2 E_2}$$

$$\varepsilon_{eff} = \varepsilon_1 - \frac{3 x_2 \varepsilon_1 (\varepsilon_1 - \varepsilon_2)}{3 \varepsilon_1 - x_1 (\varepsilon_1 - \varepsilon_2)}$$

Maxwell – Garnett formula
(1904)

$$x_2 << x_1$$

Another (re-written) form:

$$\varepsilon_{eff} = \varepsilon_1 (1 - \frac{x_2}{1-N}) + \varepsilon_2 \frac{x_2}{1-N} \frac{\varepsilon_1}{\varepsilon_1 + N(\varepsilon_2 - \varepsilon_1)}, N = \frac{1}{3}(1 - x_2)$$

Relative volume $V_1 < x_1$ of the percolated part of the matrix (not influenced by E_{dep})

Non-percolated part V_{12} of both particles and the matrix with a changed response influenced by E_{dep}

Generalised depolarization factor

$(0 \le N \le 1)$

There is no percolated cluster of particles. It can be easily generalised to ellipsoidal particles with different N.

Bruggeman theory – effective medium approximation (EMA) (1935)

The same approach as Maxwell - Garnett, but the spherical particles are embedded into a matrix with ε_{eff} instead of $\varepsilon_1 \Rightarrow$ in principle can be used for arbitrary concentration x_2:

$$x_2 \frac{\varepsilon_1 - \varepsilon_{eff}}{\varepsilon_1 + 2\varepsilon_{eff}} + x_1 \frac{\varepsilon_2 - \varepsilon_{eff}}{\varepsilon_2 + 2\varepsilon_{eff}} = 0$$

This implicit quadratic formula for ε_{eff} is symmetrical in both indices i and displays percolation threshold for the i-th component properties for $x_i = 1/3$.
It can be also generalised to n components and to ellipsoidal particles (with different depolarization factor and percolation threshold along the three principal axes of the ellipsoid).

Coated spheres model (Hashin-Shtrikman 1962)

$$\varepsilon_2 \text{ (volume } x_2 = 1 - x_1)$$
$$\varepsilon_1 \text{ (volume } x_1)$$

$$\varepsilon_{eff} = \varepsilon_1 + \frac{3(1-x_1)\varepsilon_1(\varepsilon_2 - \varepsilon_1)}{3\varepsilon_1 + x_1(\varepsilon_2 - \varepsilon_1)}$$
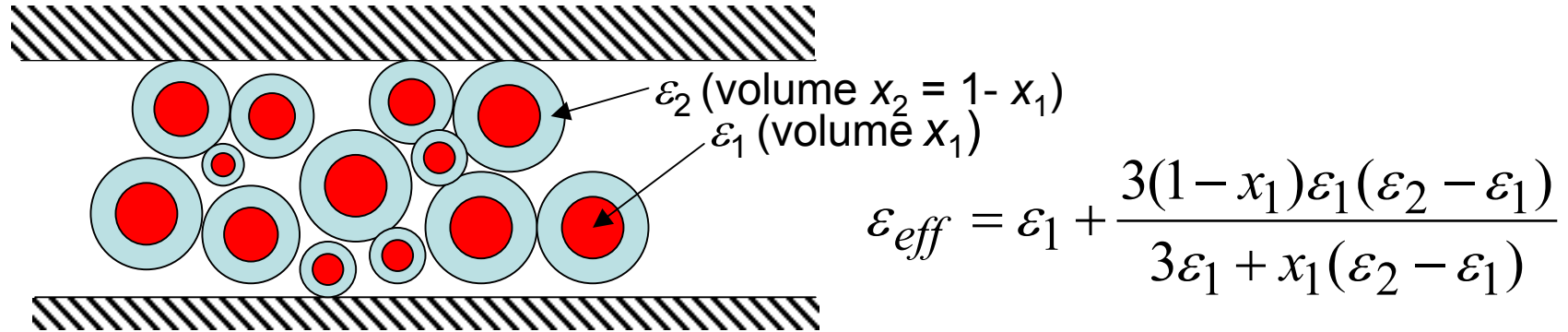
The whole volume of composite is filled up by coated spheres of all sizes from some maximal size down to zero. This model is exactly analytically solvable for any x_1. Again, $\boldsymbol{E}_{dep}$ is homogeneous. It can be again re-written into the form:

$$\varepsilon_{eff} = \varepsilon_1(1 - \frac{x_2}{1-N}) + \varepsilon_2 \frac{x_2}{1-N} \frac{\varepsilon_1}{\varepsilon_1 + N(\varepsilon_2 - \varepsilon_1)}, \quad N = \frac{1}{3}(1 - x_2)$$

Both formulas have the same form as for Maxwell - Garnett model, but the role of ε_1 and ε_2 is interchanged. There is no percolation of particles even for x_1 close to 1 (small x_2). For this case the model is also equivalent to another model when coated spherical particles are embedded into the effective medium (analogy to EMA) and to so called **brick - wall model** (with cubic bricks).

Brick - wall model
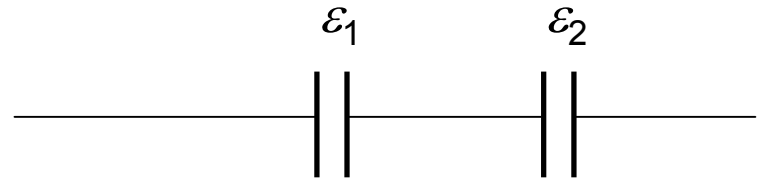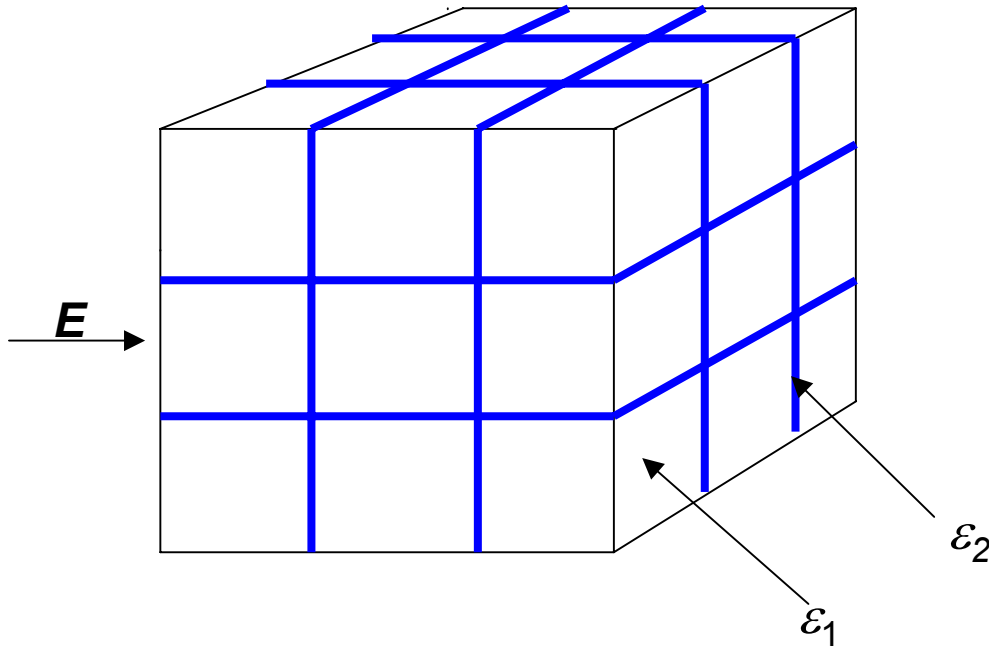
$$\varepsilon_{eff}^{-1} = x_1 \varepsilon_1^{-1} + g x_2 \varepsilon_2^{-1}$$

Equivalent circuit of series capacitors with a geometrical factor $0 < g < 1$

For cubic bricks g = 1/3, for columnar bricks g = 1/2

E_{dep} is inhomogeneous

The model is approximate, cannot be calculated rigorously, but is frequently used for ceramics to consider different properties of grain bulk and boundaries .

Upper and lower bound:

It can be shown that the dielectric response of each composite with sharp boundaries among the components must lay between two limiting values:

Upper bound – maximum response: equivalent circuit of parallel capacities, layers parallel to **E**:

$$\varepsilon_{eff} = x_1\varepsilon_1 + x_2\varepsilon_2 \qquad \boldsymbol{E}_{dep} = 0,\ N = 0,$$

Lower bound – minimum response: equivalent circuit of series capacities, layers perpendicular to **E**:

$$\varepsilon_{eff}^{-1} = x_1\varepsilon_1^{-1} + x_2\varepsilon_2^{-1} \qquad \boldsymbol{E}_{dep}\ \text{maximal},\ N = 1 - x_2$$

These formulas are independent on the thickness and number of individual layers (capacitors), only on the total relative volume of both components x_1 and x_2.

It can be shown that coated spheres model represent the upper and lower bound for an isotropic composite.

Bergman representation (1978)

Any two component composite with sharp boundaries can be written in the form (Hudak et al., 1998, Rychetsky 2004):

$$\varepsilon_{eff} = \varepsilon_1 V_1(x_1) + \varepsilon_2 V_2(x_2) + \int_0^1 V_{12}(N, x_2) \frac{\varepsilon_1 \varepsilon_2}{(1-N)\varepsilon_2 + N\varepsilon_1} dN$$

$V_i(x_i) \le x_i$ is the percolated volume of the i–th component, i =1,2

This part of the response is not influenced by $\boldsymbol{E}_{\text{dep}}$ – weighted sum of bulk responses

$$V_{12}(N, x_2) = \frac{x_2}{1-N} G(N, x_2)$$ is the non-percolated volume of both components, which depends on particle shape as well as on their concentration

spectral density function

Normalisation condition: $V_1 + V_2 + \int_0^1 V_{12} dN = 1$

All known mixing formulas can be obtained by an appropriate choice of V_1, V_2 and the $G(N,x_2)$ function.

If one could assume that $\qquad G(N,x_2) = \delta(N'-N)G_1(N)$

and one component is not percolated at all ($V_i = 0$ for $i = 1$ or 2),

the formula simplifies to (generalised brick-wall model):

$$\varepsilon_{eff} = \varepsilon_2 V_2(x_2) + V_{12} \frac{\varepsilon_1 \varepsilon_2}{(1-N')\varepsilon_2 + N'\varepsilon_1}$$

with $\quad V_1 = 0, V_2 = 1 - \dfrac{1-x_2}{1-N'}, V_{12} = \dfrac{1-x_2}{1-N'}, 0 < N' < x_2$

Only 2 free parameters x_2 and N' can be fitted from the experiment. This formula is valid for any form of particles with a single N' with arbitrary size as long as **E** is homogeneous in individual particles. Brick - wall and coated spheres models are recovered for small x_2.

High-frequency phenomena, AC response

All the formulas can be applied even for discussion of the effective dynamics, i.e. calculation of the effective dielectric function, as long as the **E** homogeneity condition is fulfilled. This in real cases goes up to the IR range including polar phonon absorption.

Let us assume the dielectric function of component in 1 the product form of generalised damped harmonic oscillators:

$$\varepsilon_1(\omega) = \varepsilon_{1,\infty} \prod_j \frac{\omega_{LOj}^2 - \omega^2 + i\omega\gamma_{LOj}}{\omega_{TOj}^2 - \omega^2 + i\omega\gamma_{TOj}} = \varepsilon_{1,\infty} + \sum_j \frac{g_j + i\omega\alpha_j}{\omega_{TOj}^2 - \omega^2 + i\omega\gamma_{TOj}}$$

If $\alpha_j = 0$, it reduces to a sum of classical damped harmonic oscillators.

Let us assume that in the frequency range of our interest the component 2 has small dispersionless permittivity ε_2. Then

$$\varepsilon_{eff}(\omega) = \varepsilon_\infty \prod_j \frac{\tilde{\omega}_{LOj}^2 - \omega^2 + i\omega\tilde{\gamma}_{LOj}}{\tilde{\omega}_{TOj}^2 - \omega^2 + i\omega\tilde{\gamma}_{TOj}} = \varepsilon_\infty + \sum_j \frac{\tilde{g}_j + i\omega\tilde{\alpha}_j}{\tilde{\omega}_{TOj}^2 - \omega^2 + i\omega\tilde{\gamma}_{TOj}}$$

The renormalised effective transverse mode parameters to the first approximation assuming $x_2 \ll x_1$ and $\varepsilon_2 \ll \varepsilon_1$ are

$$\widetilde{\omega}^2_{TOj} = \omega^2_{TOj} + \frac{N' g_j}{\varepsilon_2} = \omega^2_{TOj}\left(1 + \frac{N' \Delta\varepsilon^{j}}{\varepsilon_2}\right), \quad \widetilde{\gamma}_{TOj} = \gamma_{TOj} + \frac{N' \alpha_j}{\varepsilon_2}$$

while the longitudinal mode parameters (eigenfrequencies and dampings) remain unchanged.

The shift up of $\widetilde{\omega}^2_{TOj}$ with respect to ω^2_{TOj} increases linearly with x_2 and N' and the dielectric strength $\Delta\varepsilon^{j}$ but it always remains below the next longitudinal-mode frequency. The effective mode strengths are reduced:

$$\widetilde{\Delta\varepsilon}_j \approx \Delta\varepsilon_j\left(1 - N'\frac{\Delta\varepsilon_j}{\varepsilon_2} - N'\sum_{k \neq j}\frac{\Delta\varepsilon_k / \varepsilon_2}{1 - \omega^2_{TOj} / \omega^2_{TOk}}\right)$$

Similar formulas and conclusions are valid also for dielectric relaxations: the effective relaxation frequencies are increased and dielectric strengths reduced.

If we release the assumption of zero percolation of component 1, all these renormalised modes appear in addition to un-renormalised (weaker) modes due to percolated clusters of component 1. The renormalised modes are usually called "geometrical resonances" (Fröhlich modes or surface modes in case of isolated particles).

If also the component 2 has a dielectric function with poles (polar modes), additional modes un-shifted (corresponding to percolated clusters) and shifted-up (corresponding to non-percolated clusters) appear in the effective dielectric function. Also the longitudinal-mode frequencies are modified. So generally the dielectric function of a 2-component composite consists of twice the number of modes in both components.

If also the assumption of single N' is released, instead of each single geometrical resonance we obtain an absorption continuum – smearing of the shifted-up transverse modes. This can be easily seen from the general Bergman formulation.

Examples: Simple perovskites ABO$_3$ ceramics and films – SrTiO$_3$, PbZrO$_3$ and BaTiO$_3$

A

B

O^{-2}

(a)

(b)
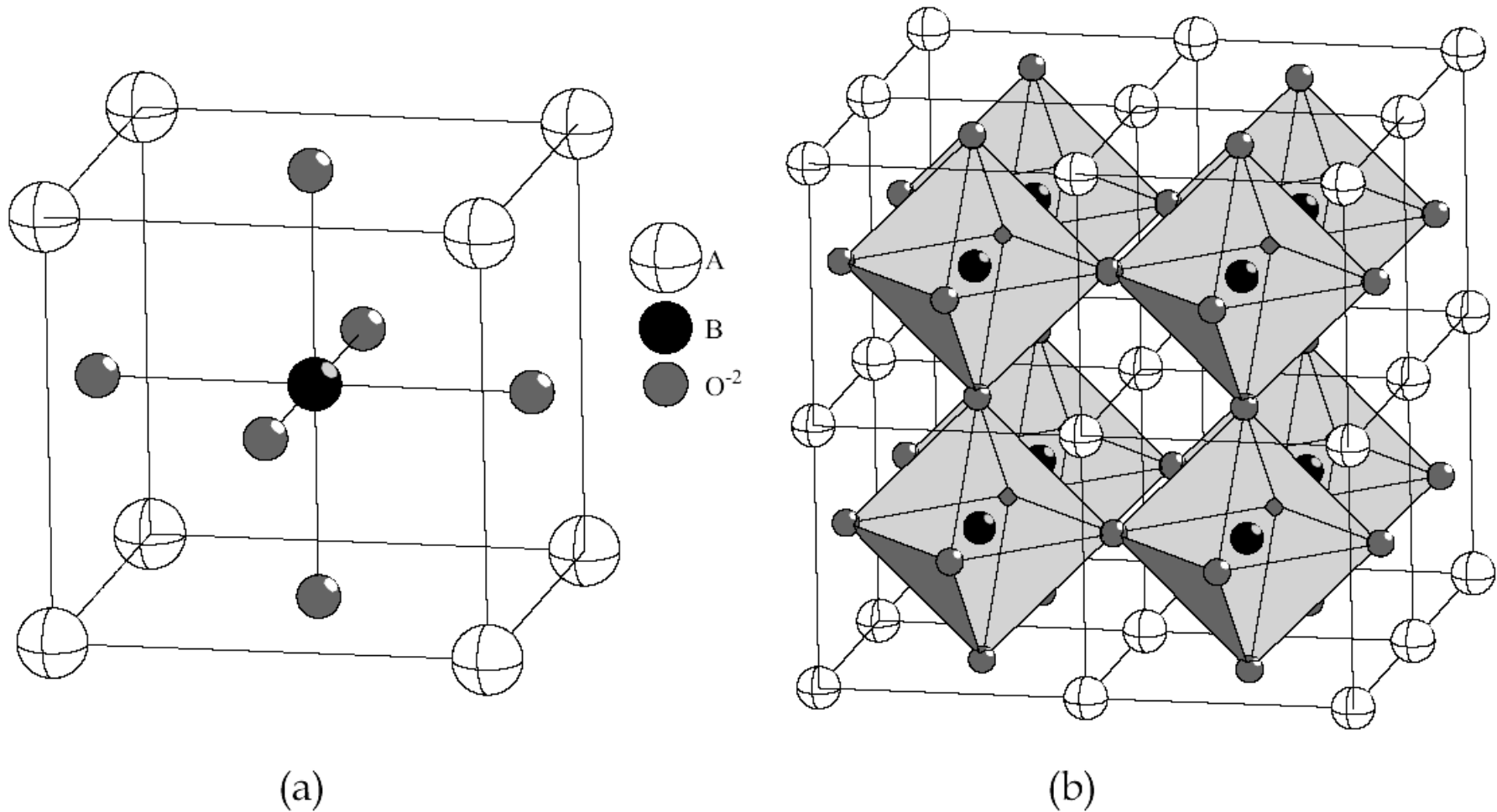
Figure 4. 1 The cubic ABO$_3$ structure (a) unit cell and (b) octahedra framework.

SrTiO$_3$ (STO)

Incipient ferroelectric, at 105 K antiferrodistortive transition from simple cubic
Pm3m structure to tetragonal phase I4/mcm in the R-point of the Brillouin zone

Splitting of the
structural soft
mode
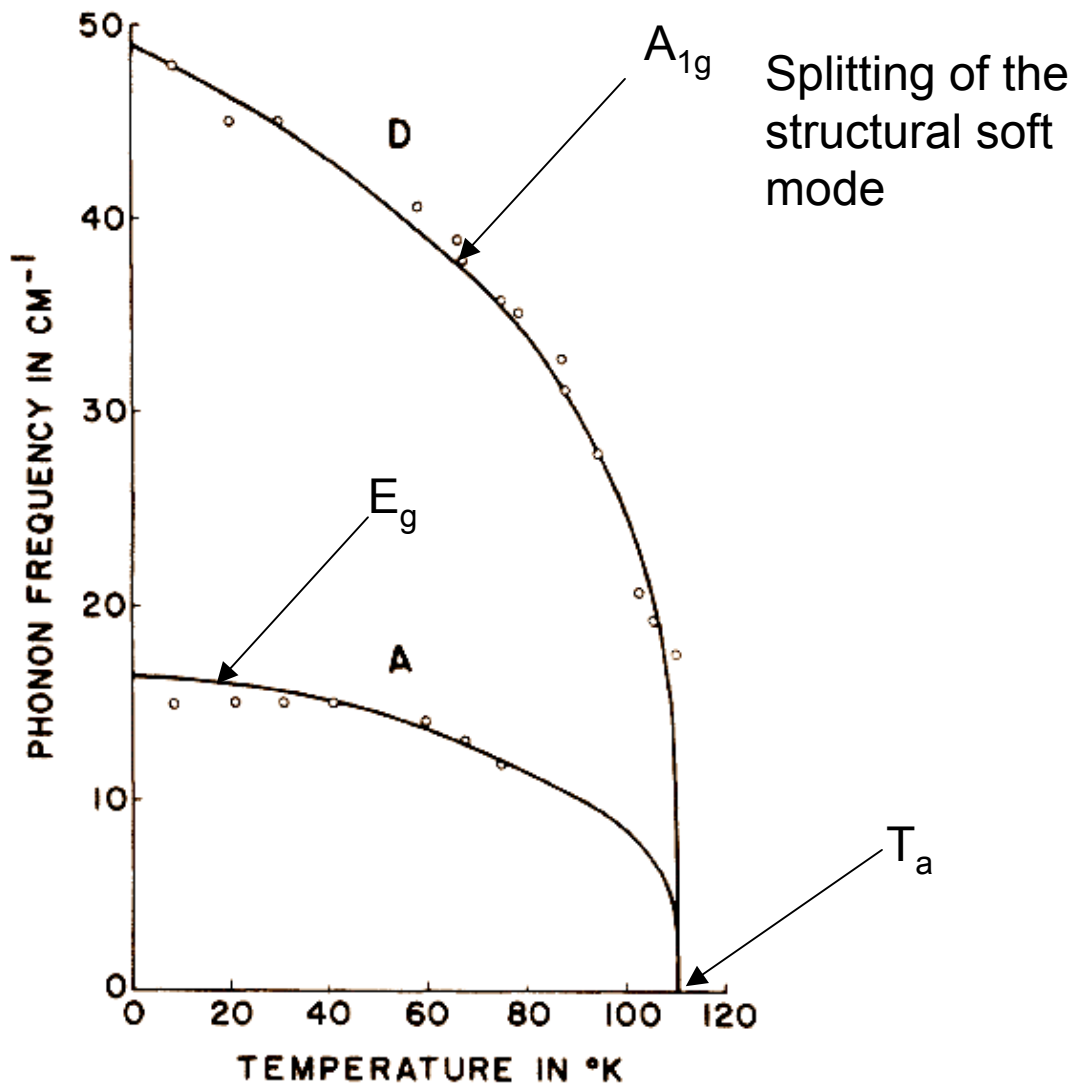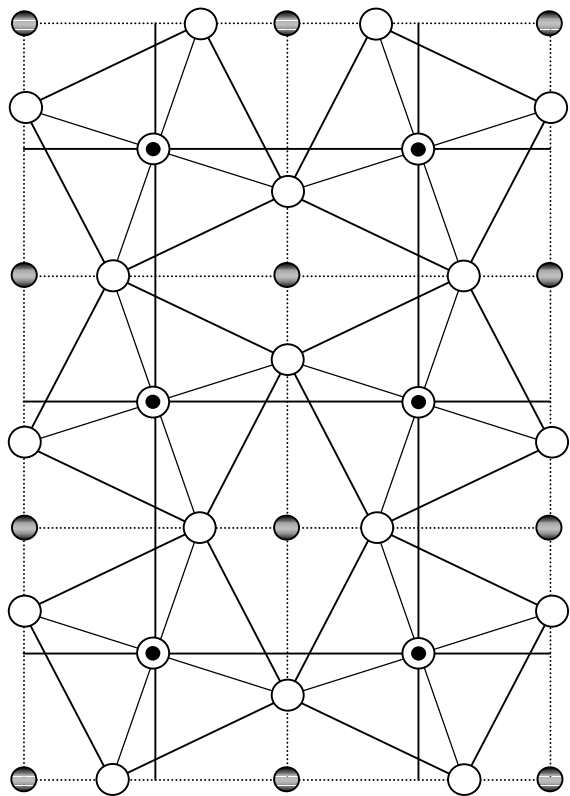
Anisotropy of permittivity and splitting of the ferroelectric soft-mode in $SrTiO_3$ below the antiferrodistortive transition
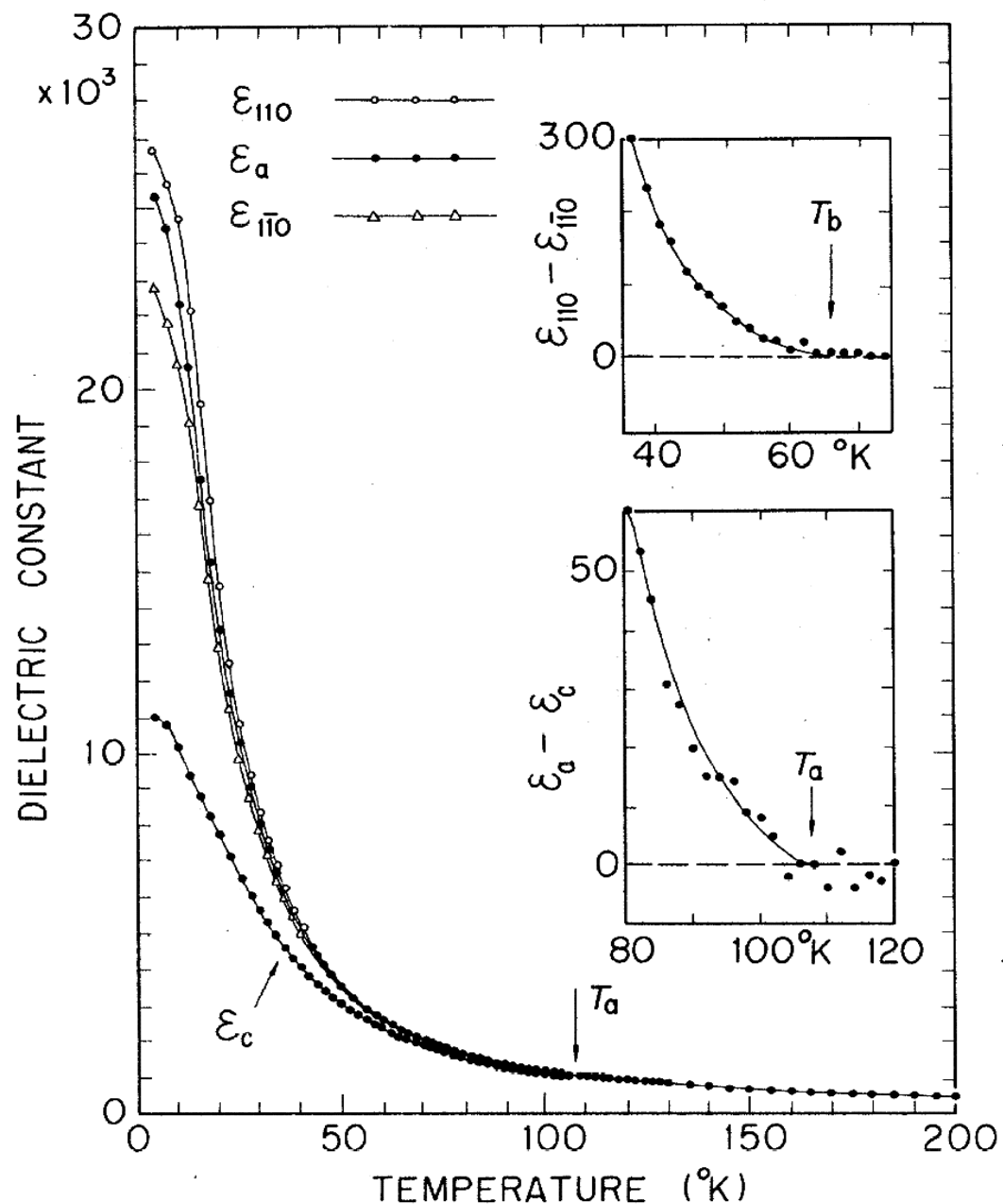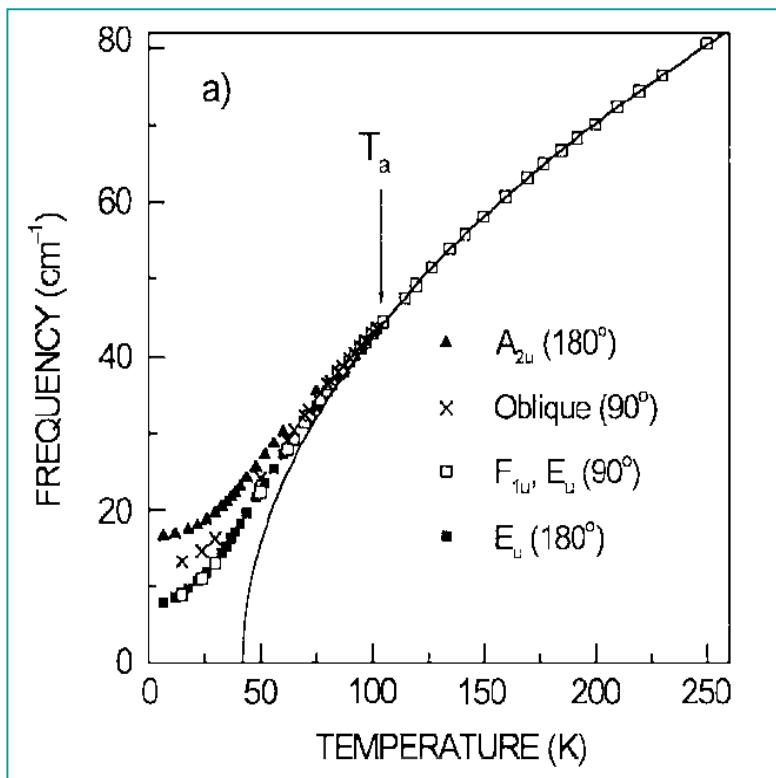
Factor-group analysis of the lattice vibrations and observed modes in the STO ceramics:

Ferroelectric SM

Structural SM (doublet)

Mode frequencies on STO ceramics

(Petzelt et al., PRB **64**, 184111 (2001))

species	activity	observed	species	activity	observed
$Pm\bar{3}m$ (O_h^1) $Z = 1$ ($P_S=0$, T=300 K)			$I4/mcm$ (D_{4h}^{18}) $Z_{prim}=2$ ($P_S=0$, T=15 K)		
$3F_{1u}$	IR	93,176,548	$3A_{2u}$ $3E_u$	IR	15,172,548
$1F_{2u}$	HR	266	$1B_{2u}$ $1E_u$	- IR	- -
$1R'_{15}(F_{1g})$	N	~40 (soft)	$1A_{1g}$ $1E_g$	R	52 40
$2R'_{25}(F_{2g})$	-	-	$2B_{1g}$ $2E_g$	R	144,447
$1R_{15}(F_{1u})$	-	-	$1A_{1u}$ $1E_u$	- IR	- 436
$1R_{12}(E_g)$	-	-	$1A_{2g}$ $1B_{2g}$	- R	- 229
$1R_1(A_{1g})$	-	-	$1A_{2g}$	-	-
Total (Γ point)	$3F_{1u}+1F_{2u}$		$1A_{1g}+1A_{1u}+2A_{2g}+3A_{2u}+$ $+2B_{1g}+2B_{2g}+2B_{2u}+3E_g+3E_u$		
Mode activity	3 IR		8IR+7R		

Permittivity of STO ceramics at different frequencies and Curie-Weiss fit
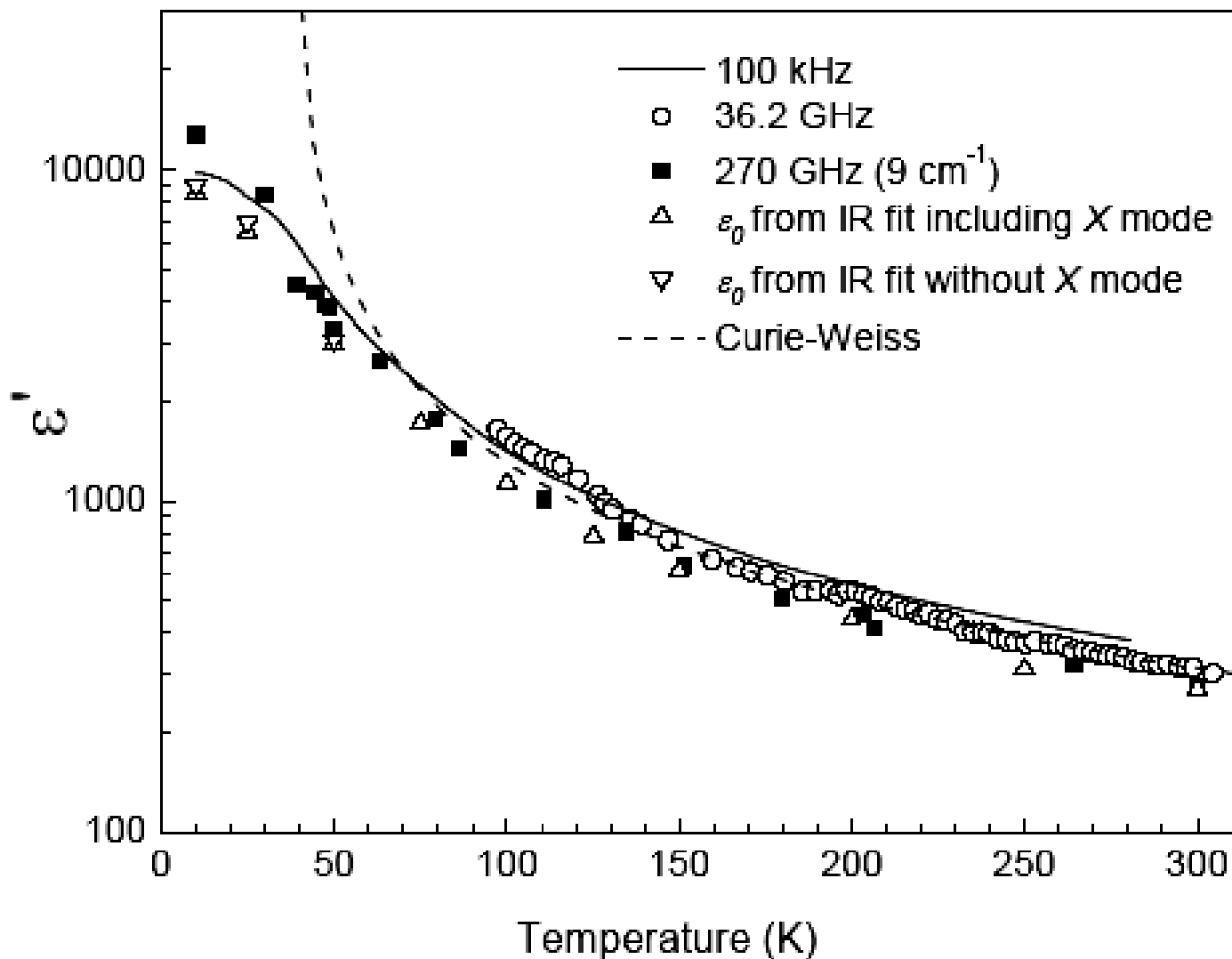
IR Reflectivity of STO ceramics:

Thin full lines – FTIR data

Thick full lines – BWO data

Full squares – calculated from BWO transmission

Dotted and dashed lines – different fits
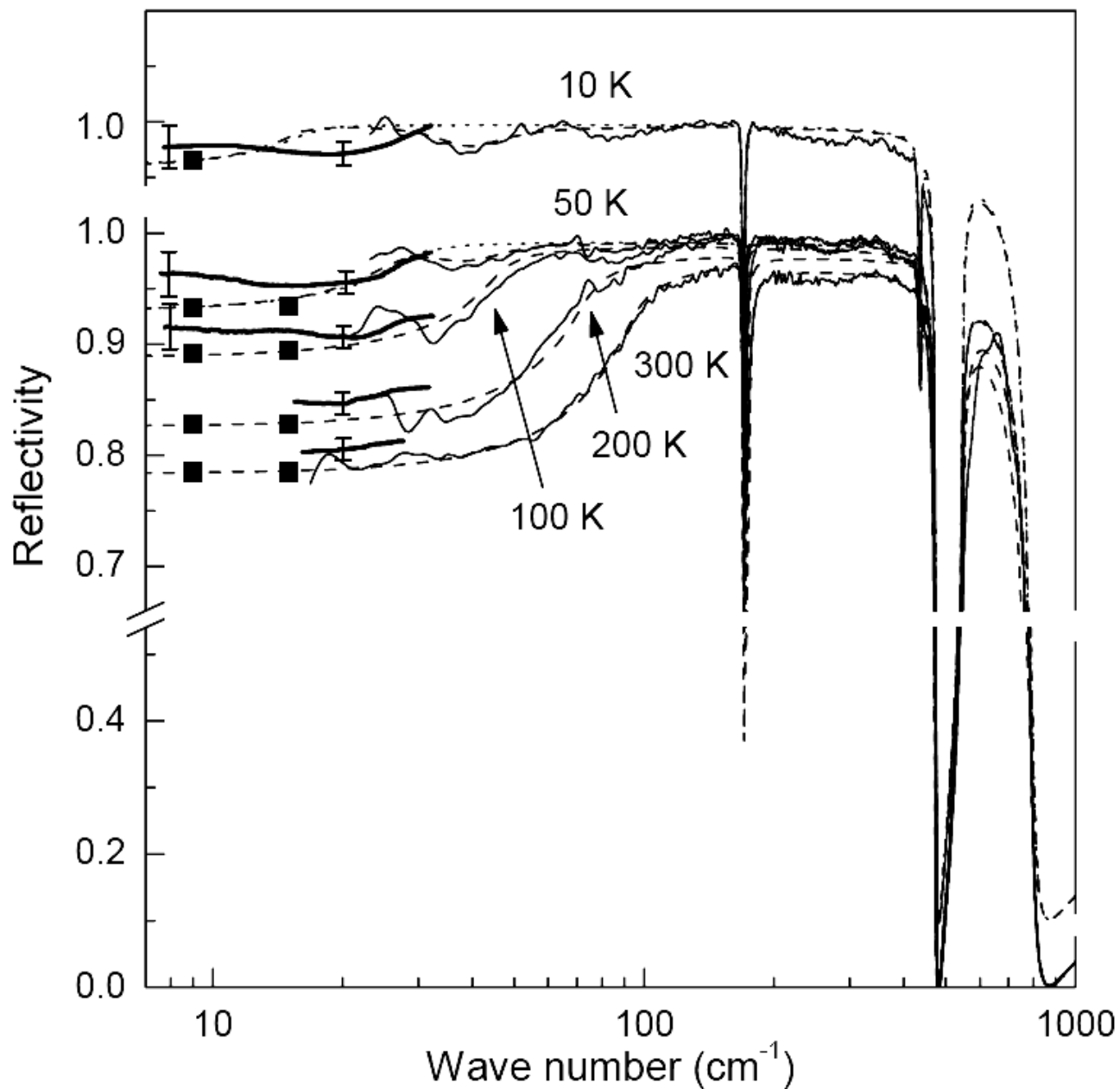
Dielectric spectrum of STO ceramics

Ferroelectric soft-mode eigenvector
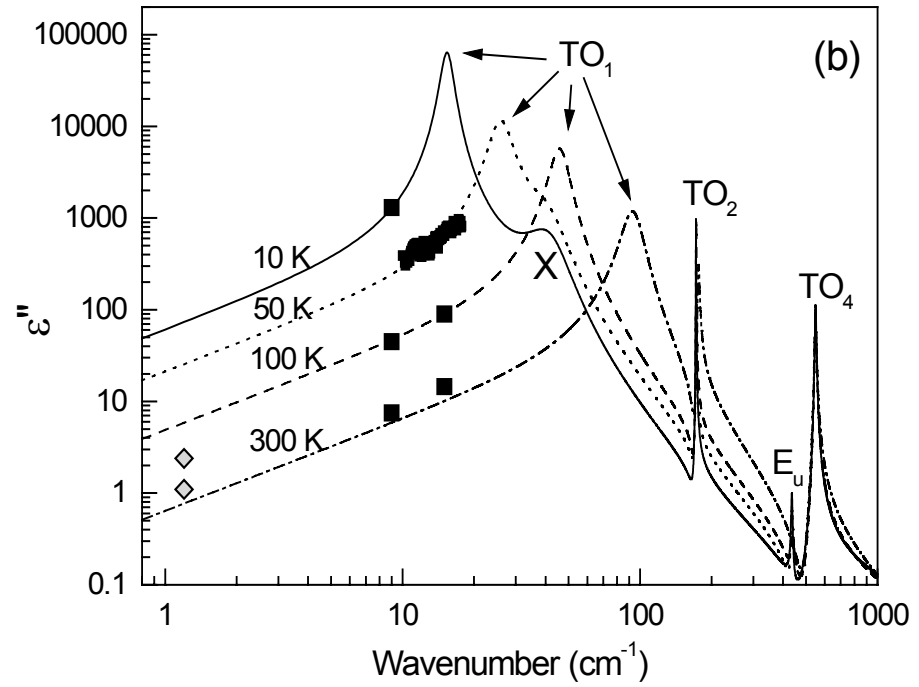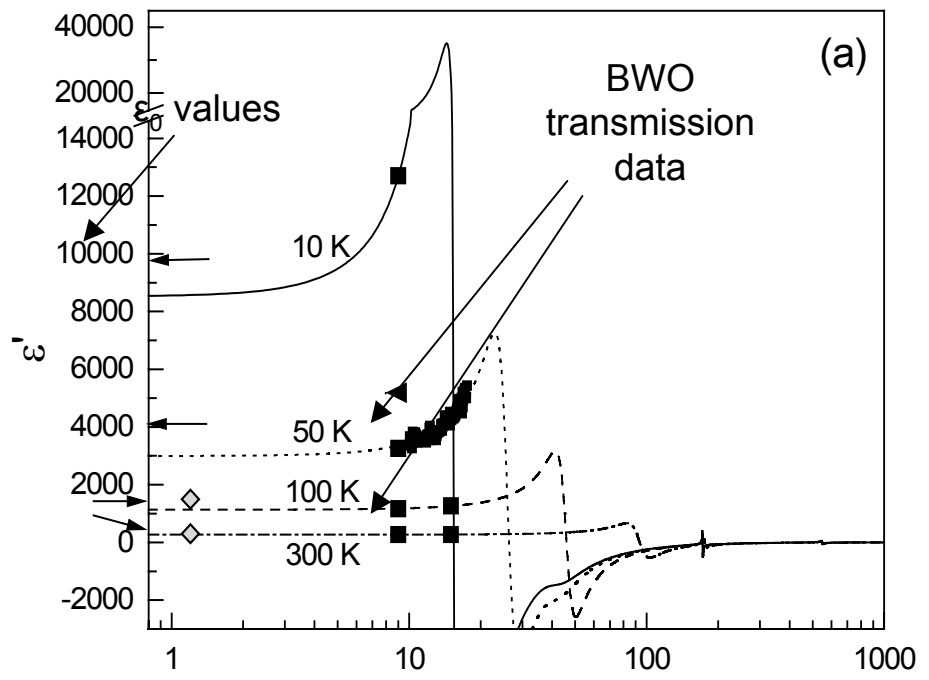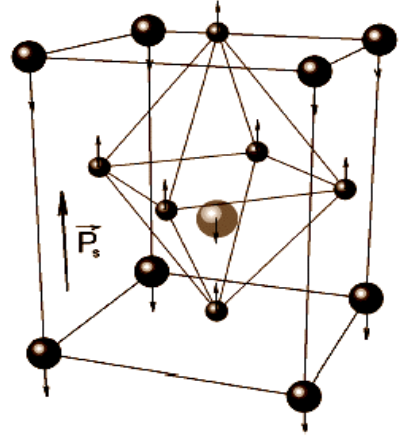
Unpolarized Raman spectra of STO ceramics
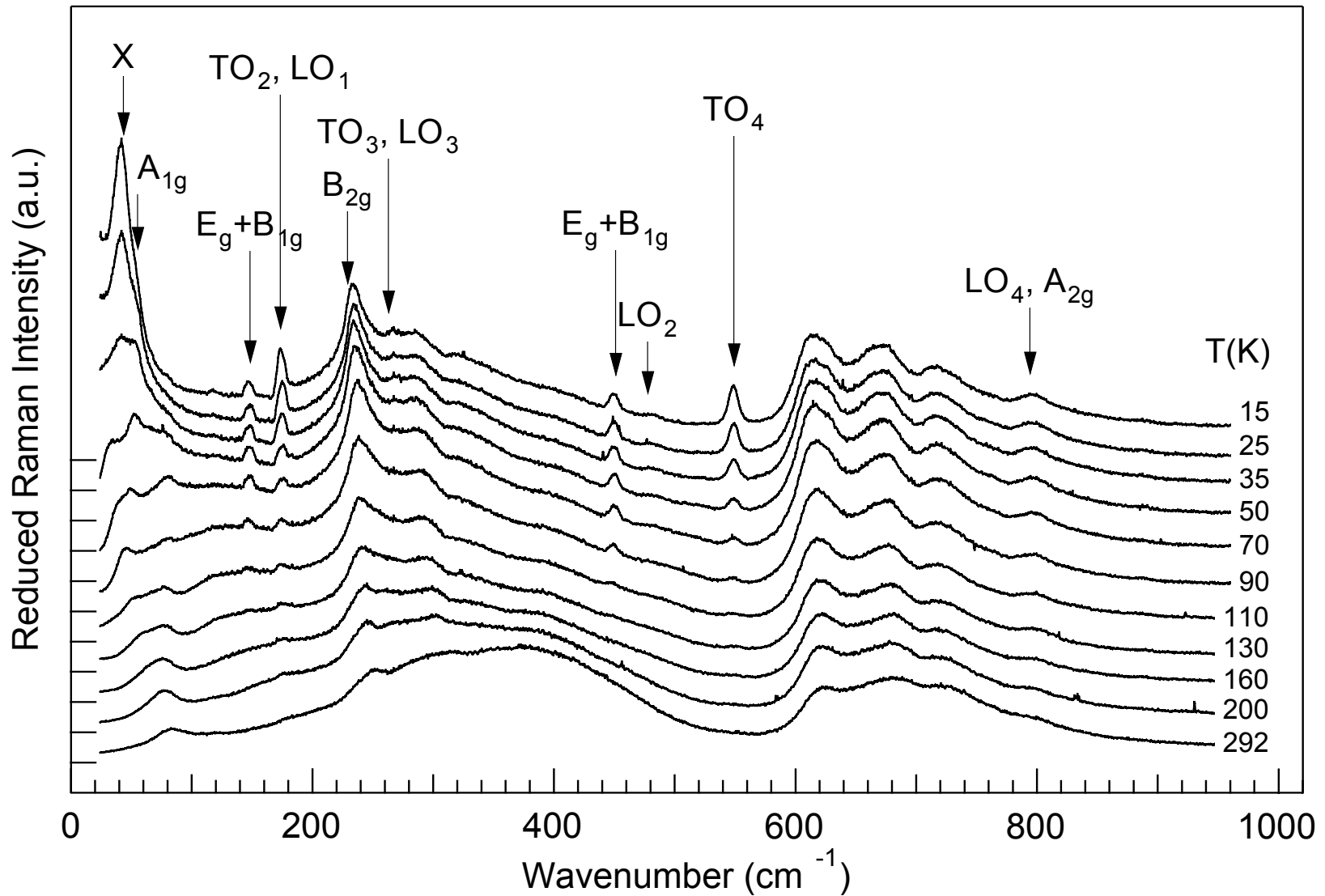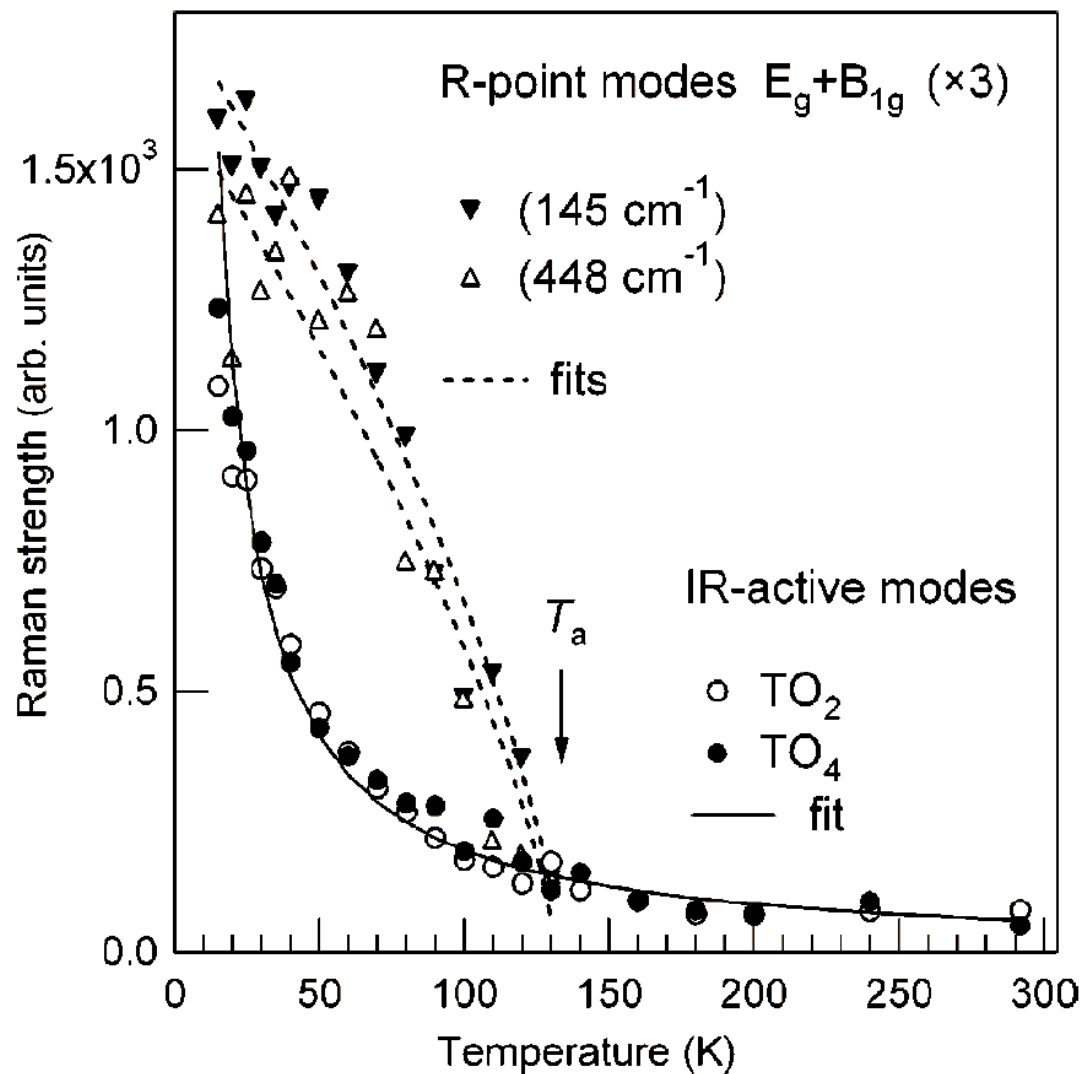
FIG. 9. Temperature dependences of the Raman strengths of the selected R-point and IR modes. The dotted lines correspond to $I \propto (T_a - T)^{0.72}$, the full line to $I \propto e^{-aT}$.

Interpretation:

Assume existence of frozen grain-boundary dipole moment. This interface polarization P_{gb} penetrates inside the thin slabs with the penetration (correlation) length ξ proportional to $\varepsilon^{1/2}$ or ω_{SM}^{-1} (theory by Rychetsky and Hudak, 1997). In the case of dimensionality d of the polarization penetration, the average polarization is

$$\overline{P} \propto P_f \xi^d$$

Raman strength of IR modes (assuming incoherent scattering of individual grains) is

$$I_R \propto \overline{P} \propto P_f \xi^d \propto 1/\omega_{SM}^d$$

Our experiment yields $d \approx 1.6$ in a good qualitative agreement with expectations.

Correlation between the Raman strength of forbidden IR modes with the SM frequency: $I_R \propto \omega_{SM}^{-1.6}$
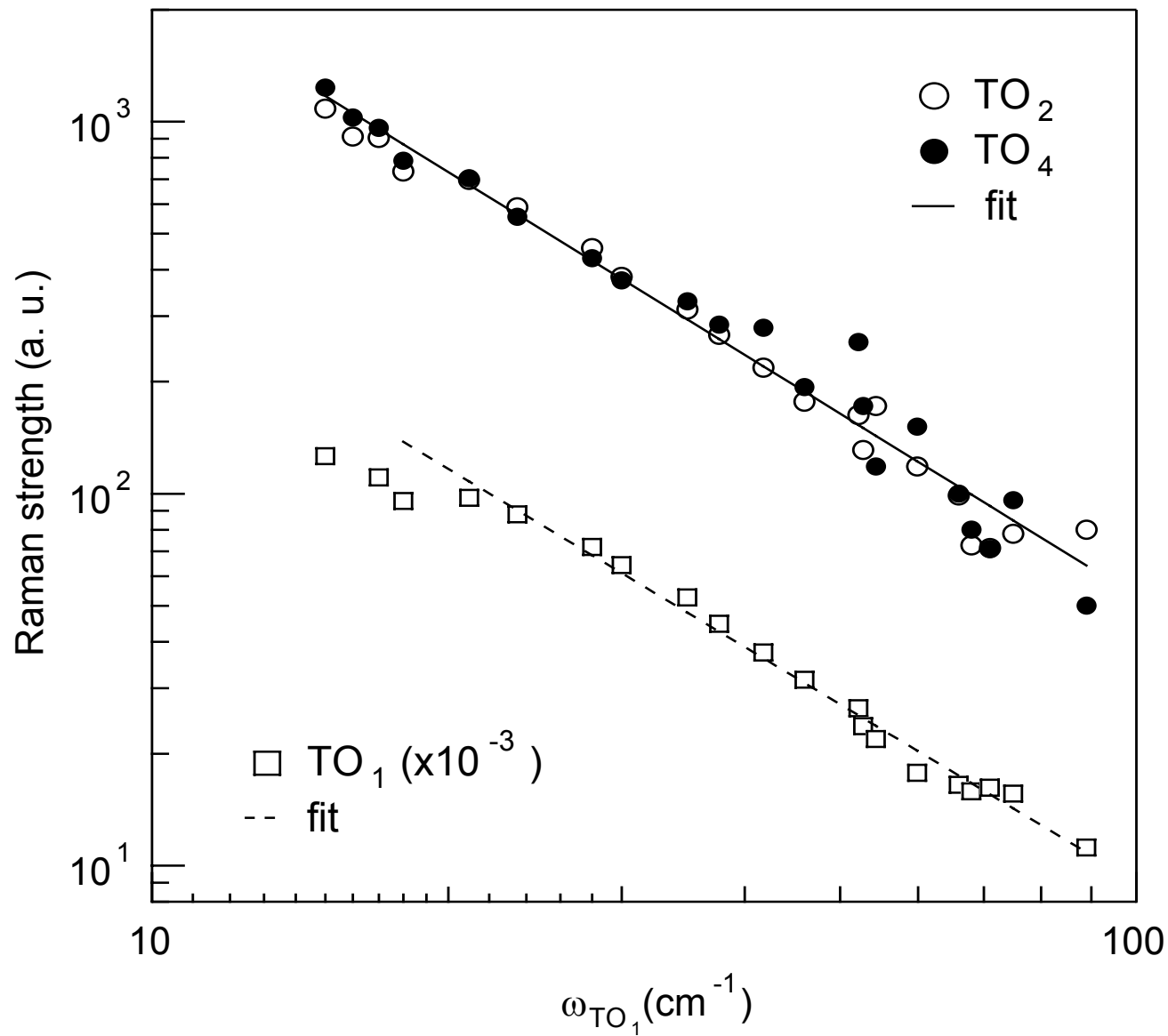
Optic mode frequencies detected in STO ceramics

Differences with respect to single crystal data concern only the low-frequency and low-T data for both SMs

(Petzelt et al., PR**B 64**, 184111 (2001))

Structural SM doublet

Ferroelectric SM
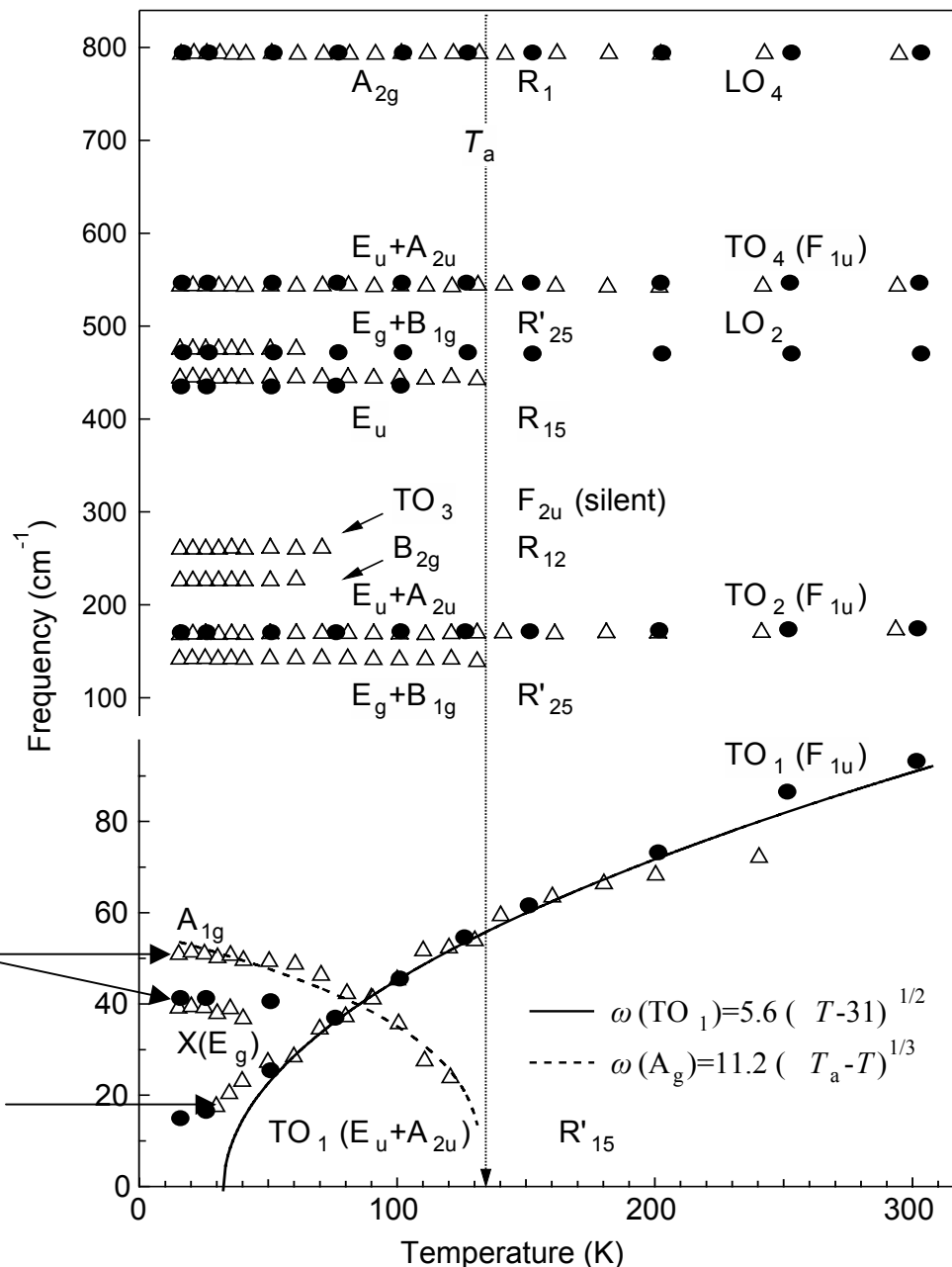
Quasi-epitaxial MOCVD STO film on (0001) sapphire substrate
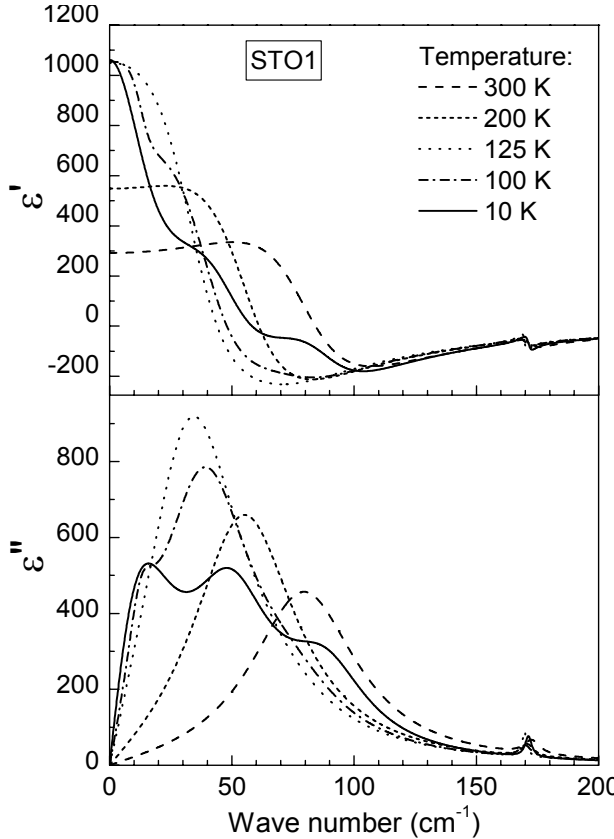
Real and imaginary part of dielectric function of STO1 film at selected temperatures, obtained from the fit of the transmittance spectra.
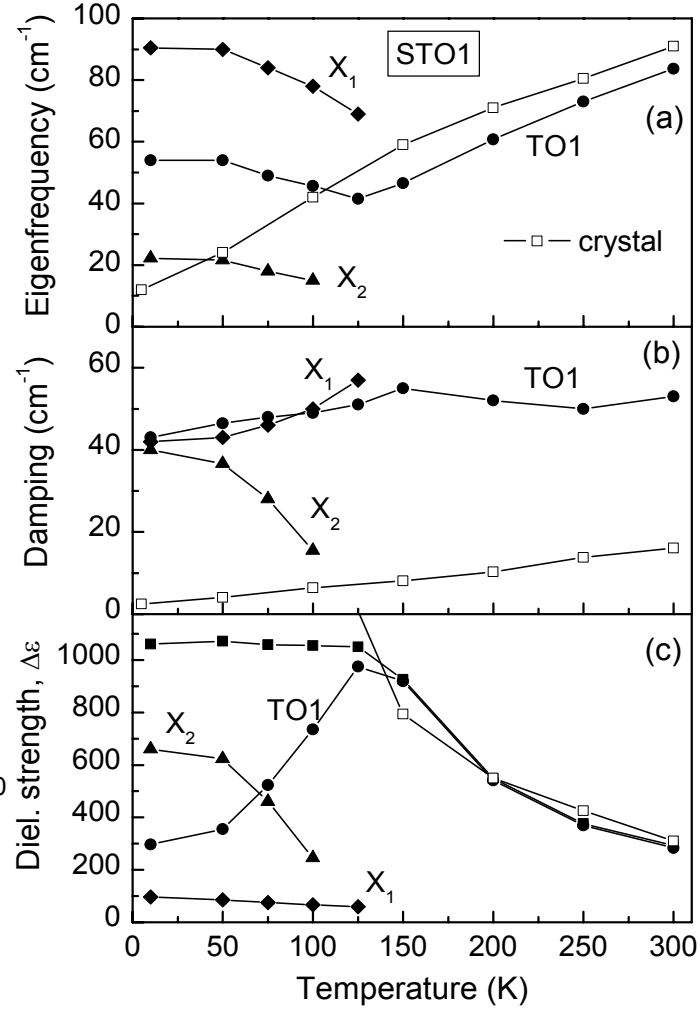
Temperature dependence of the fit parameters of the lowest IR modes in a STO1 film in comparison with the parameters of TO1 mode in a single crystal

Coupled mode fit of the SM frequencies in STO1 film.

ω_0, ω_1, ω_2 – bare frequencies, full symbols - measured coupled frequencies

α_1 – real coupling constant between the ferroelectric SM and A_1-component of the structural SM

α_2 – real coupling constant between the ferroelectric SM and E-component of the structural SM

No dielectric strength assumed for the bare structural SM doublet.
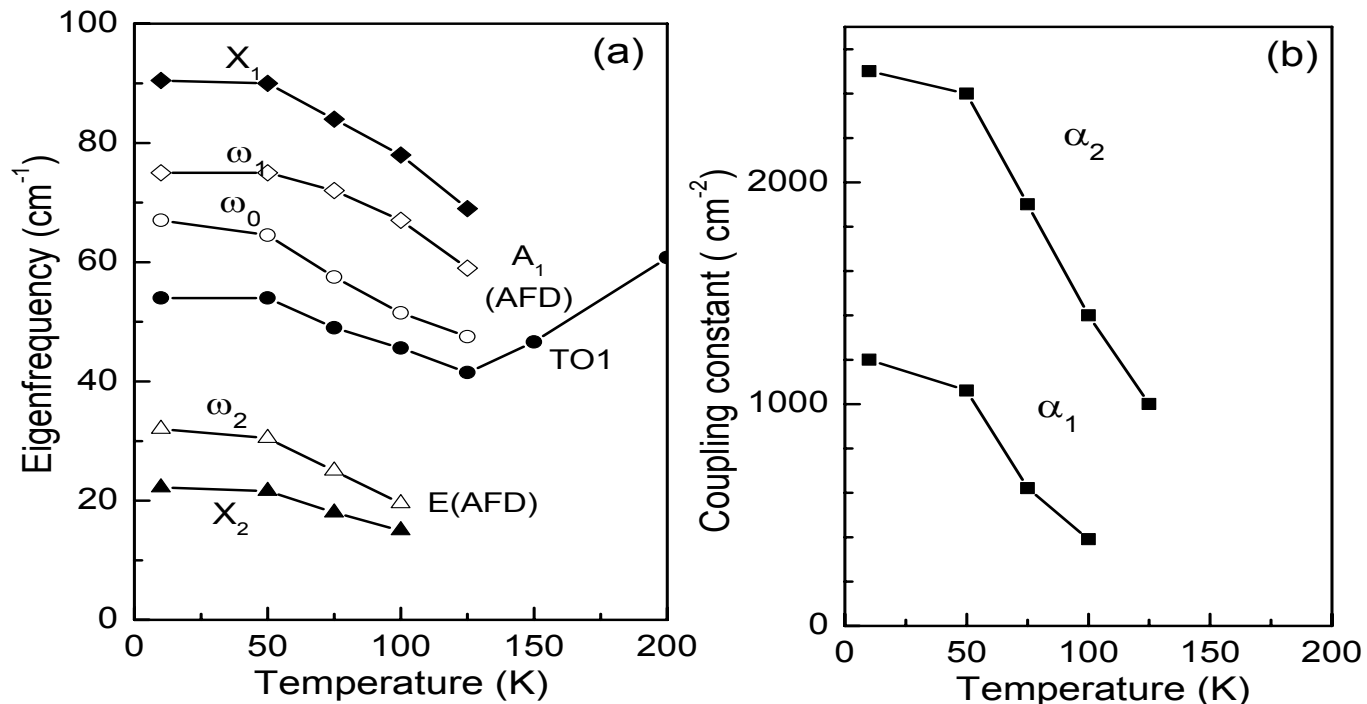
STO1 – forbidden IR modes seen only below the structural transition

STO3 – polycrystalline CVD film: forbidden IR modes seen up to 300 K
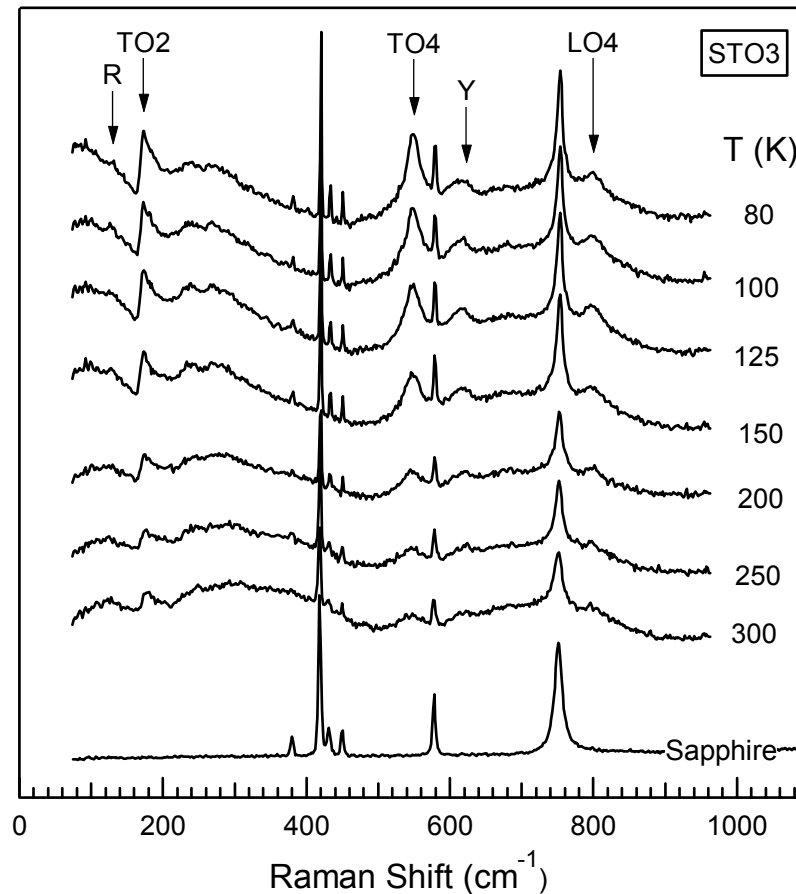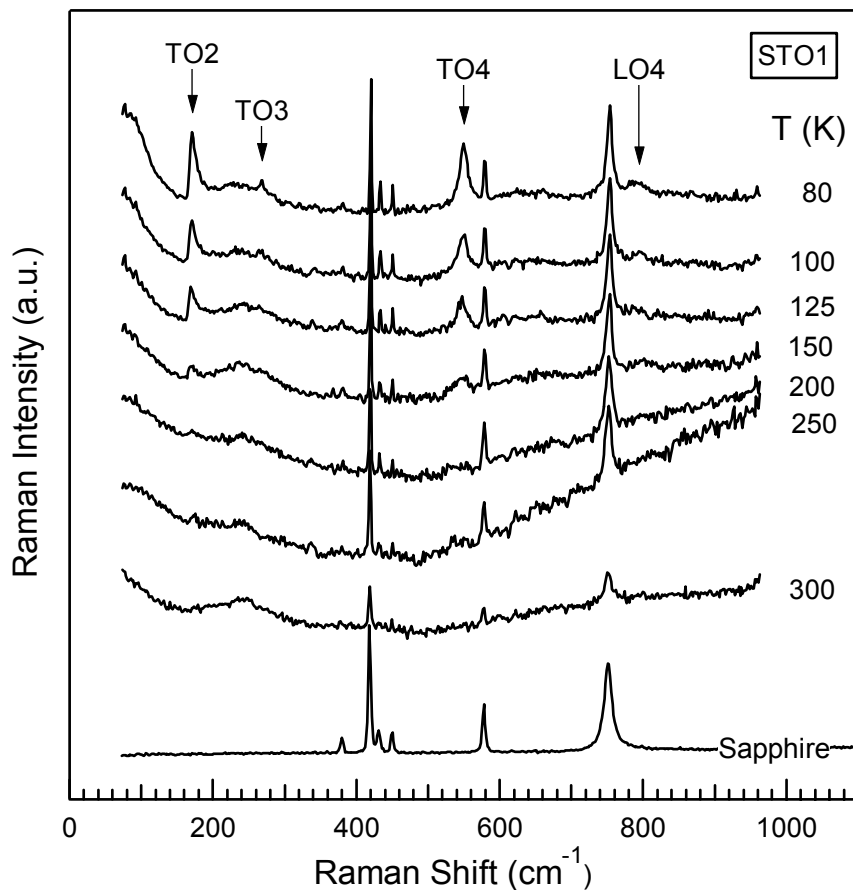
Micro-Raman spectra of STO1 and STO3 films at selected temperatures.
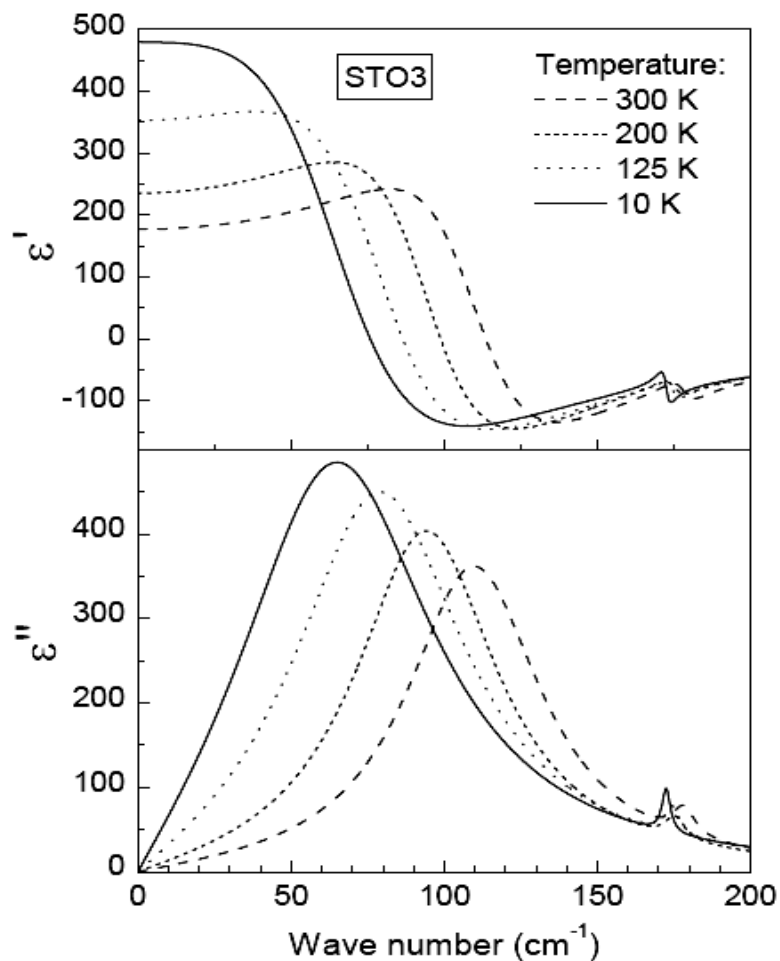
Figure 3.15. Real and imaginary part of the dielectric permittivity of a STO3 film at selected temperatures, obtained from the fit of the transmittance spectra.
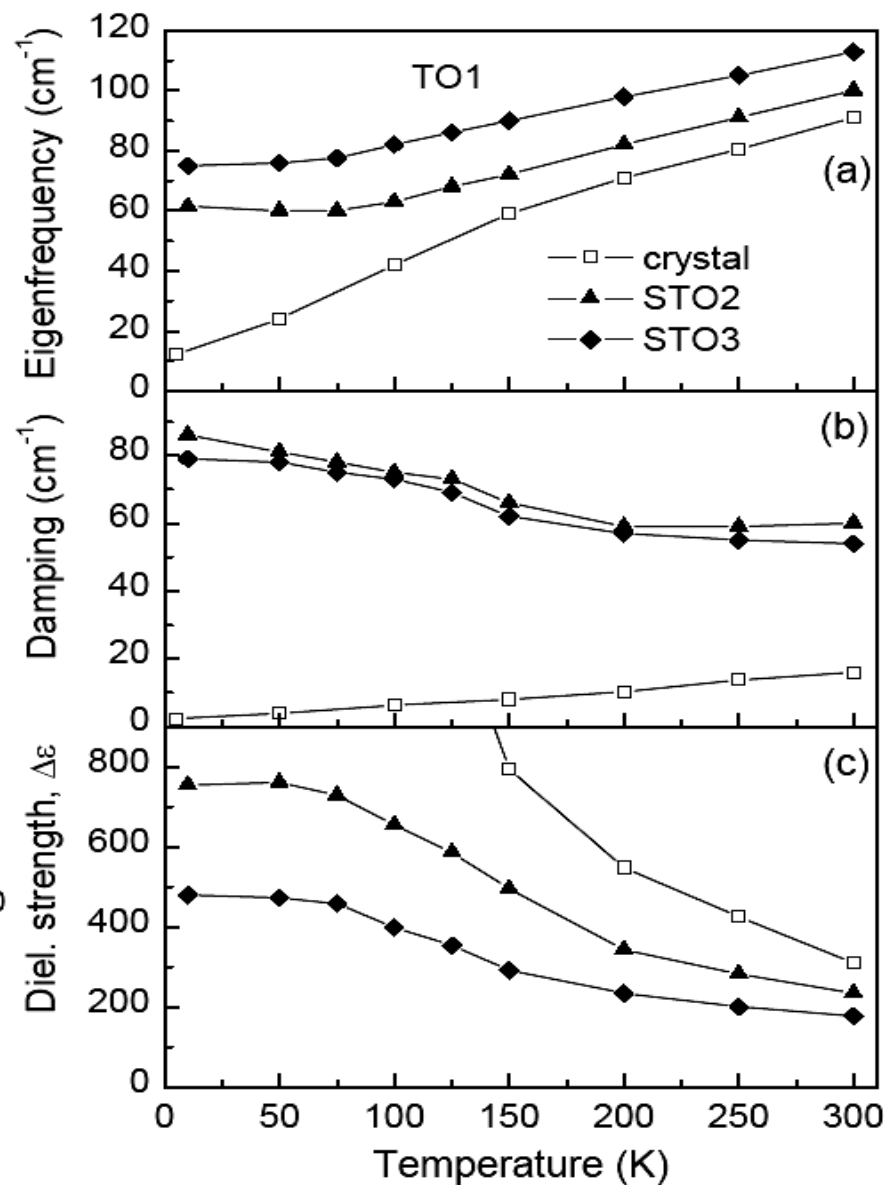
Figure 3.16. Temperature dependence of the fit parameters of the TO1 modes in STO2 and STO3 films in comparison with corresponding parameters in a single crystal [FEDOROV_98].

SEM picture of STO3 film

x50000   500nm ⊢————————⊣   1.00kV   3mm
#940145 STO 800   IWE RWTH

(a)

50 μm

(b)

0 μm   2.5 μm   5 μm
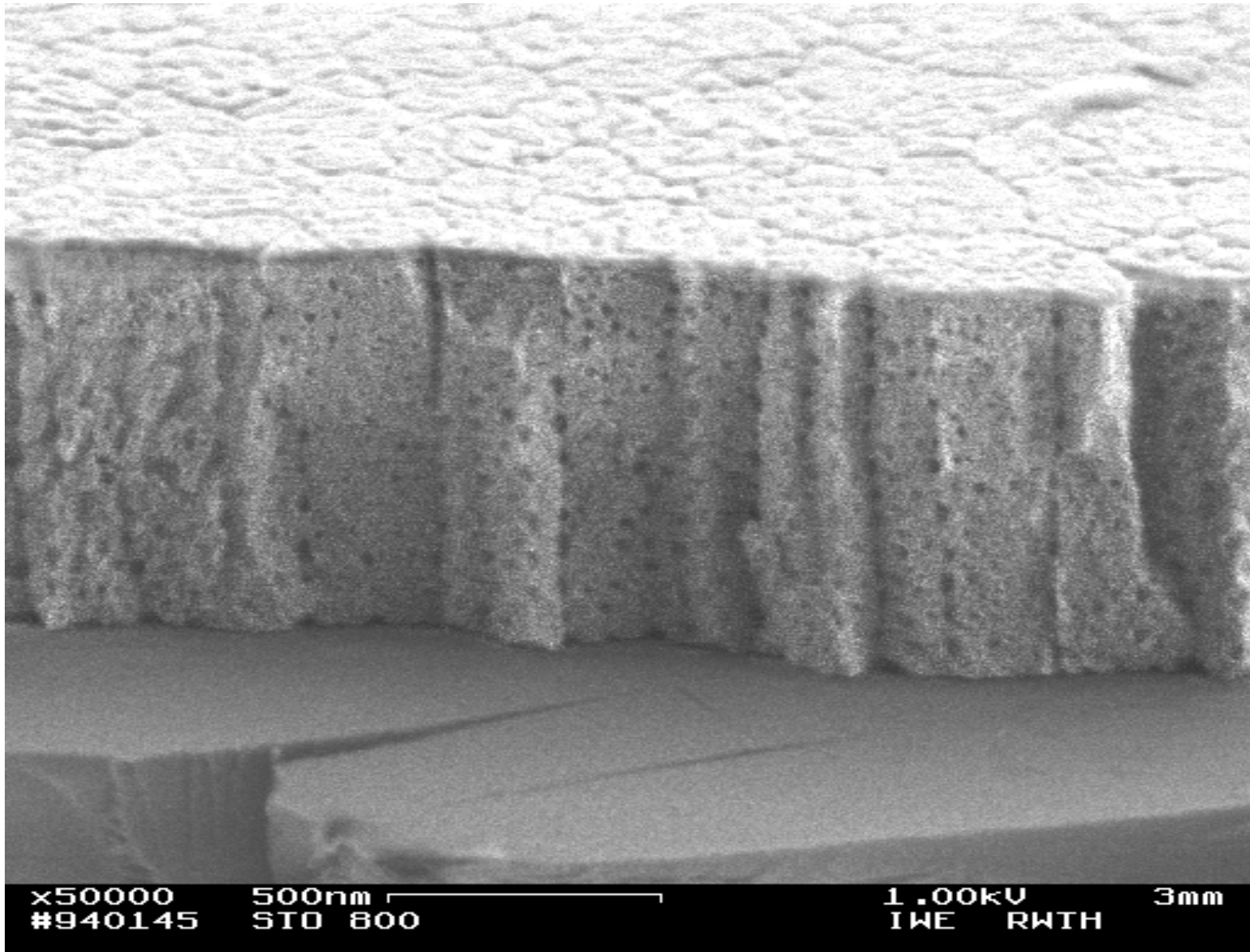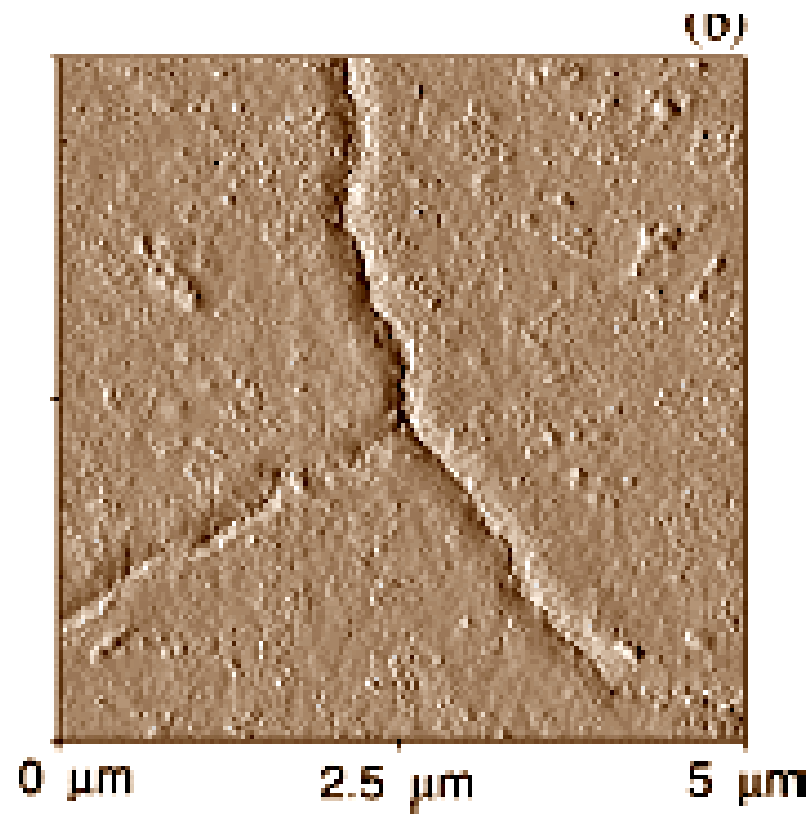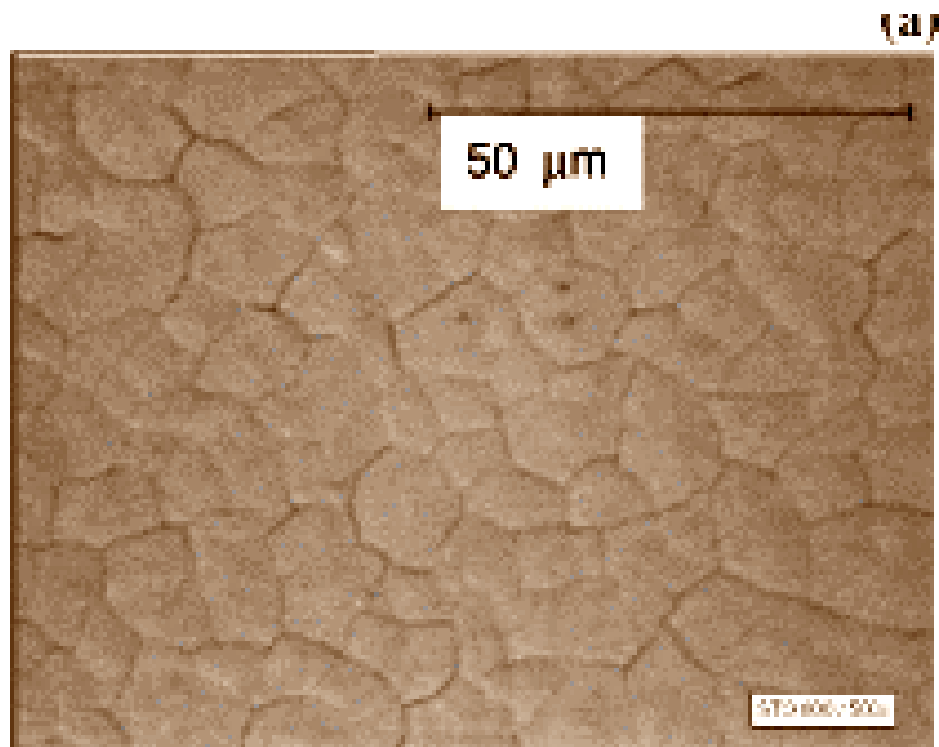
FIG. 13. Optical microscope (a) and AFM (b) views of a STO3 film surface, indicating the presence of cracks.

Brick-wall model of the effective dielectric response in a film with columnar grains and possible nano-cracks along some of the grain boundaries
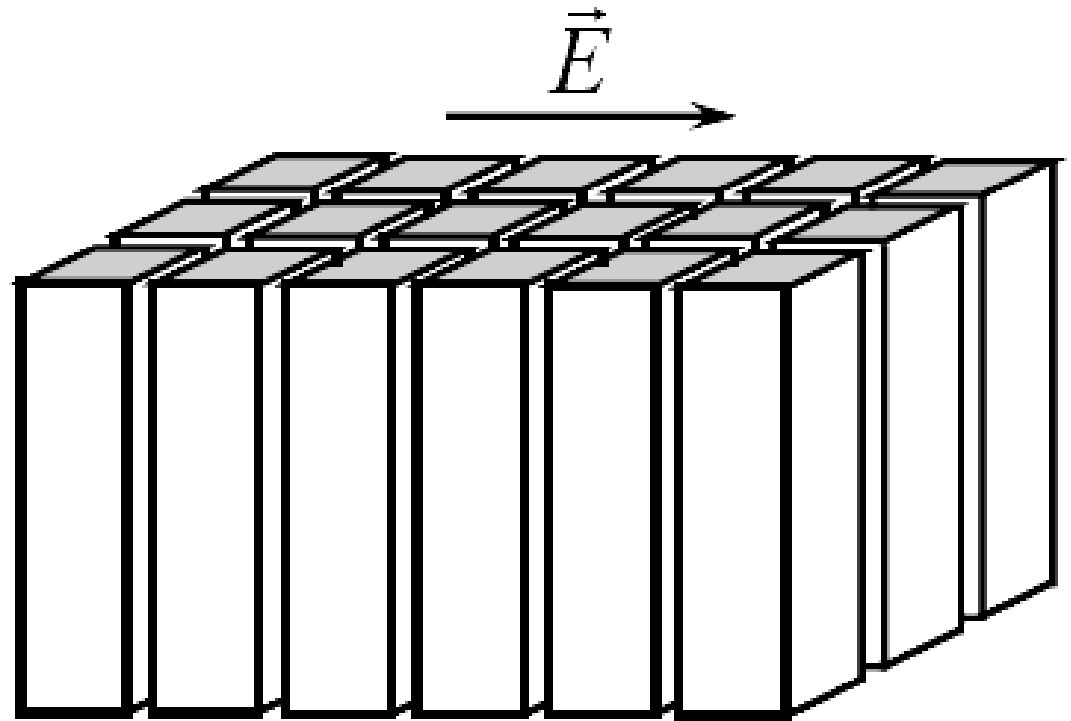
$$\frac{1}{\varepsilon_{eff}} = \frac{1 - x_{gb} - x_0}{\varepsilon_b} + \frac{g_{gb} x_{gb}}{\varepsilon_{gb}} + \frac{g_0 x_0}{\varepsilon_0}$$
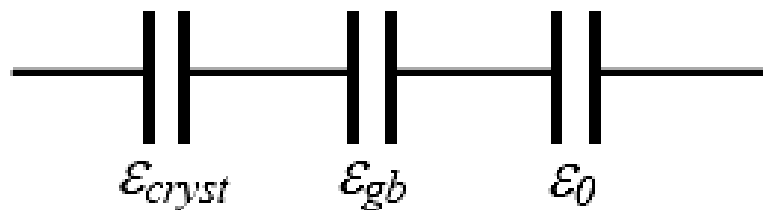
Upper and lower bound for considering the grain boundaries and porosity (cracks):

Parallel and series capacitors:

$$\varepsilon_{\text{eff}} = x_b \varepsilon_b + x_{\text{gb}} \varepsilon_{\text{gb}} + x_{\text{air}} \varepsilon_{\text{air}}, \tag{1}$$

$$\varepsilon_{\text{eff}}^{-1} = x_b \varepsilon_b^{-1} + x_{\text{gb}} \varepsilon_{\text{gb}}^{-1} + x_{\text{air}} \varepsilon_{\text{air}}^{-1}, \tag{2}$$

Grain-boundary effect neglected, only porosity p considered:

Brick-wall model:

$$\frac{1}{\varepsilon_{\text{eff}}} = \frac{1-p}{\varepsilon_b} + \frac{gp}{\varepsilon_{\text{air}}} \approx \frac{\varepsilon_{\text{air}} + gp\,\varepsilon_b}{\varepsilon_{\text{air}}\varepsilon_b}, \tag{3}$$

Coated spheres :

$$\varepsilon_{\text{eff}} = \varepsilon_{\text{air}} + \frac{1-p}{\dfrac{1}{\varepsilon_b - \varepsilon_{\text{air}}} + \dfrac{p}{3\varepsilon_{\text{air}}}}$$

$$= \frac{2p}{3-p}\varepsilon_{\text{air}} + \left(1 - \frac{2p}{3-p}\right)\frac{\varepsilon_{\text{air}}\varepsilon_b}{\left(1 - \dfrac{p}{3}\right)\varepsilon_{\text{air}} + \dfrac{p}{3}\varepsilon_b} \qquad (4)$$

Maxwell – Garnett:

$$\varepsilon_{\text{eff}} = \varepsilon_b + \frac{3p\varepsilon_b(\varepsilon_{\text{air}} - \varepsilon_b)}{3\varepsilon_b + (1-p)(\varepsilon_{\text{air}} - \varepsilon_b)} = \left(1 - \frac{3p}{2+p}\right)\varepsilon_b$$

$$+ \frac{3p}{2+p}\frac{3\varepsilon_{\text{air}}\varepsilon_b}{(2+p)\varepsilon_{\text{air}} + (1-p)\varepsilon_b}, \qquad (5)$$

Effect of porosity on the STO permittivity at 300 and 10 K

- (1) Parallel capacitors

- (2) Series capacitors

- (3) Brick-wall model

- (4) Coated-spheres model

- (5) Maxwell Garnett
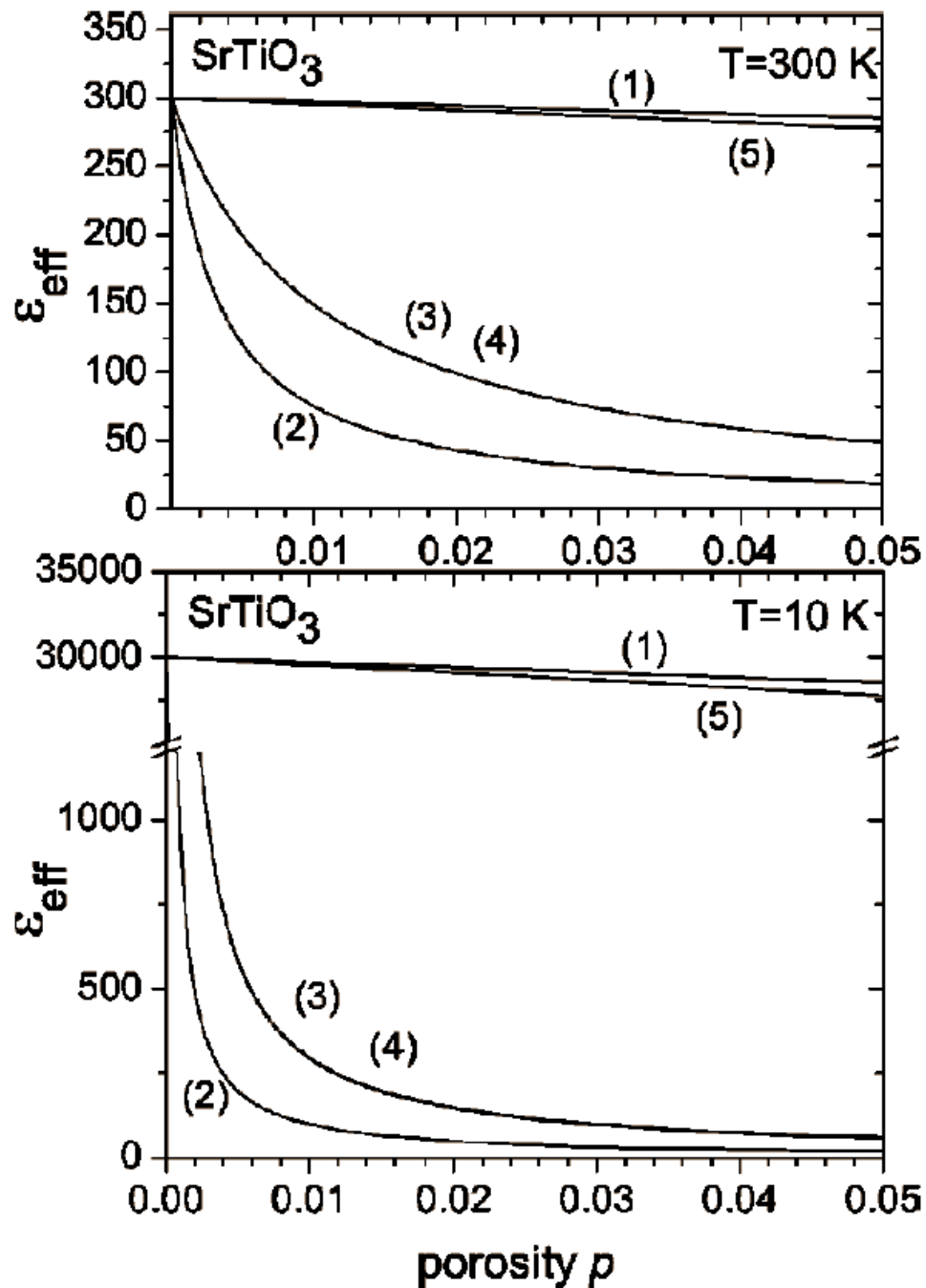
Influence of the air porosity on the effective optic mode frequencies in SrTiO$_3$ calculated according to the brick-wall model (and coated spheres model with almost identical results) in effective medium approximation.

Network of cracks of the thickness of ~5 nm and distance of ~10 µm along some of the grain boundaries.

The main effect is stiffening of the TO1 soft mode. LO frequencies are not affected.
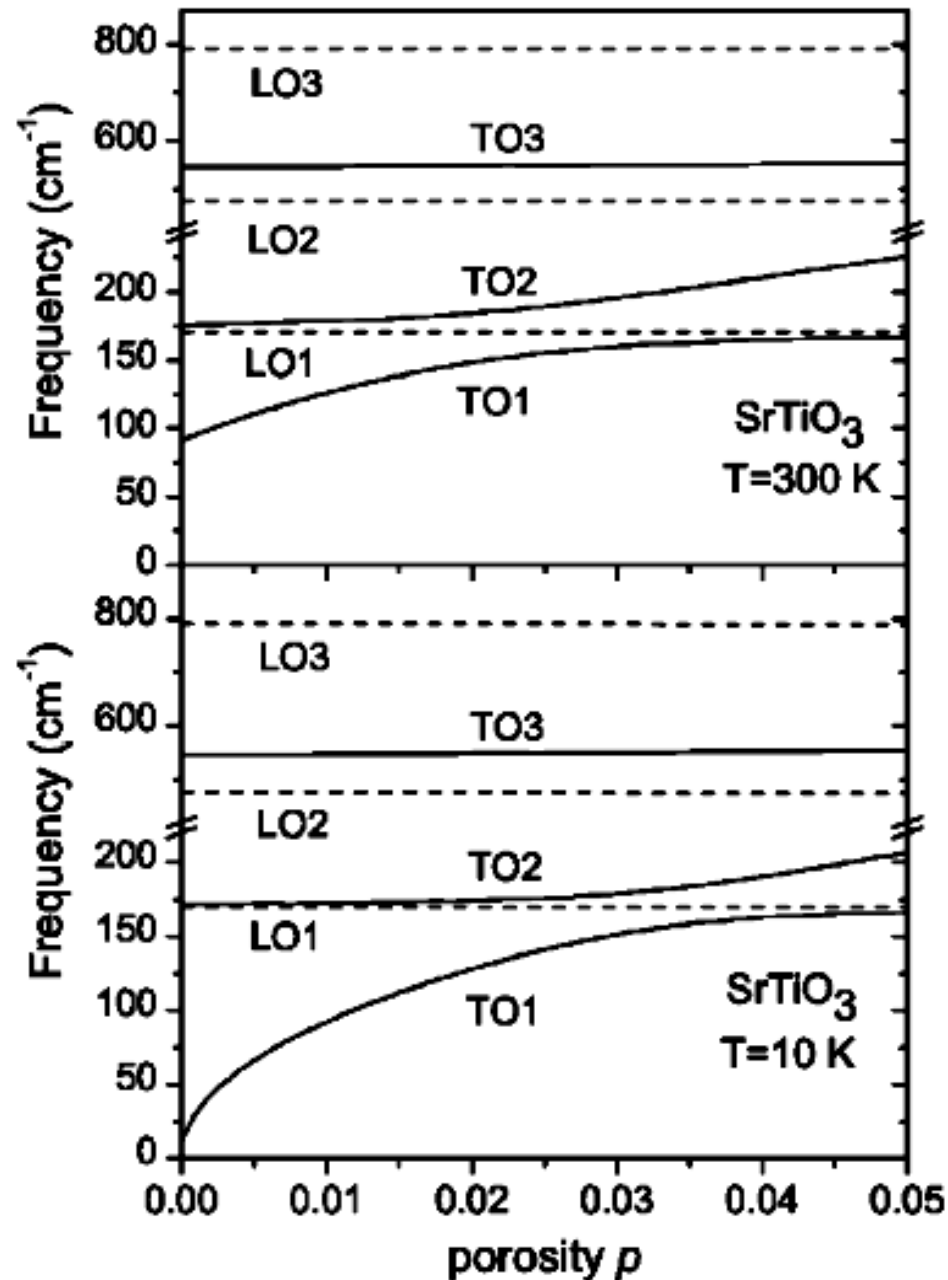
Data on STO2 and STO3 polycrystalline films can be explained assuming 0.2 vol.% and 0.4 vol.% air cracks (dominating over the effect of grain boundaries), respectively, roughly independent of temperature. These cracks release the tensile stresses which are present in the compact epitaxial film and their concentration increases with the film thickness.
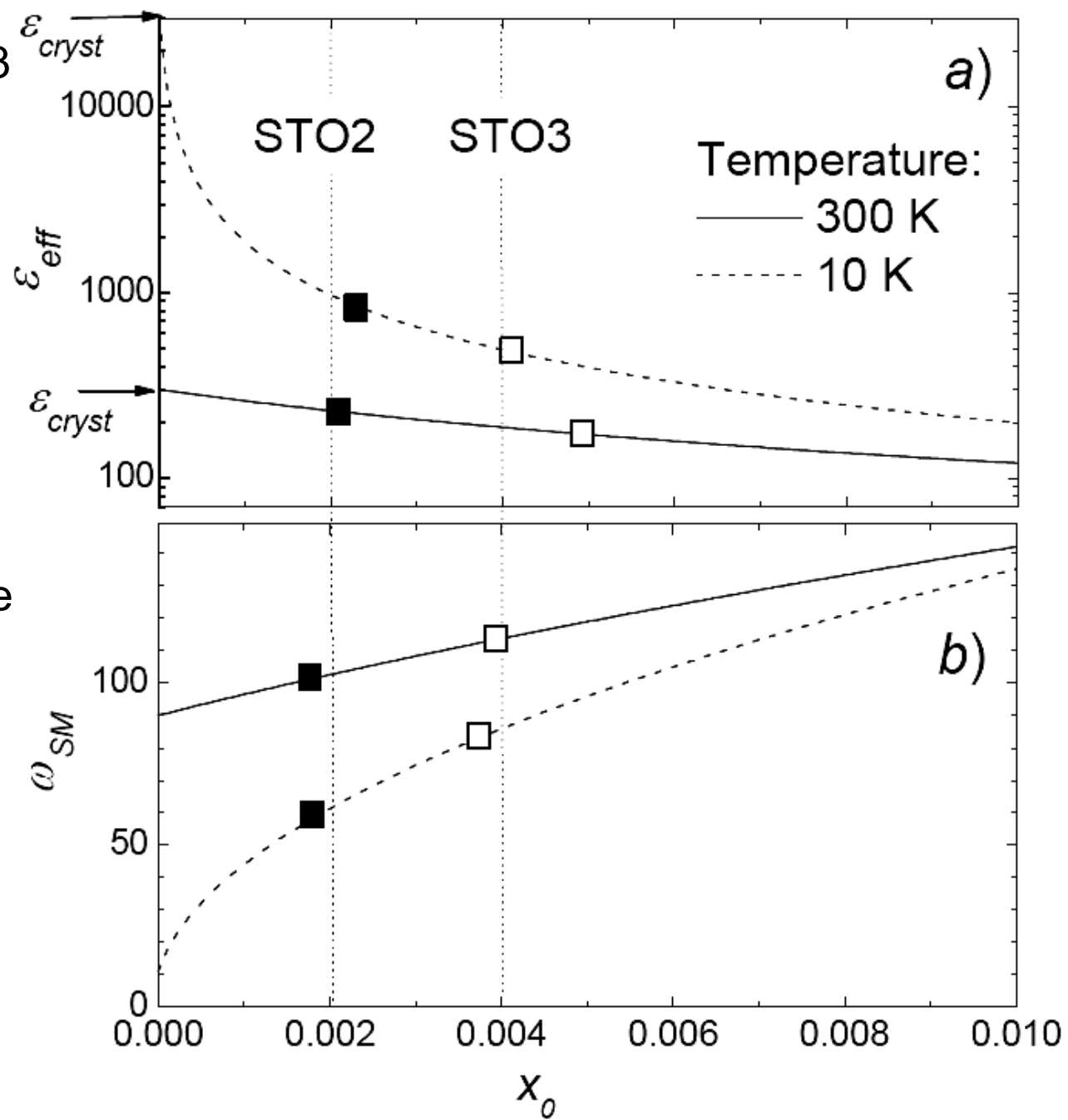
TABLE II. Structural and FE soft-mode characteristics of STO films.

No.	Deposition method	Substrate	Thickness (nm)	Sr/Ti ratio	Stress-free lattice param. a_0 (nm)	Residual in-plane stress (GPa)	Cracks	Grain structure	Soft-mode frequency (cm^{-1}) (in-plane component)			Ref.
									300 K	100 K	10 K	
1	CSD	$(1\bar{1}02)Al_2O_3$	160	1.00	-	tensile 1.5	no	100 nm, random orientation	93	60	65	31
2	CSD	$(1\bar{1}02)Al_2O_3$	180	0.83	0.39066	tensile 0.9±0.1	-	⟨110⟩ texture	95	71	72	28
3	PLD	$(1\bar{1}02)Al_2O_3$	275	-	-	-	-	⟨110⟩ texture	95	63	64	17
4	MOCVD	$(0001)Al_2O_3$	290	0.97	0.39057	tensile 0.7±0.1	no	~100 nm, ⟨111⟩ highly oriented	83	45+78	22+54+91	STO1
5	PLD	$(0001)Al_2O_3$	330	-	-	-	-	-	98	-	50+100	27
6	CSD	$(0001)Al_2O_3$	360	1.05	0.39045	tensile 0.40±0.05	no	~100 nm, weak ⟨100⟩ texture	100	63	61	STO2
7	CSD	$(1\bar{1}02)Al_2O_3$	440	0.94	-	-	yes	~100 nm, ⟨100⟩ texture	111	76	75	31
8	CSD	$(0001)Al_2O_3$	680	0.96	0.39031	tensile 0.15±0.03	yes	~100 nm, weak ⟨100⟩ texture	113	82	75	STO3
9	CSD	SiO_2 glass	70−800	-	-	-	yes	-	110	-	-	29
10	PLD	(001) MgO	90−1070	-	-	-	-	-	102	-	-	67
11	PLD	$SrRuO_3+SrTiO_3$	2000	-	-	-	-	-	99	68	62	25
	Ceramics	-	-	1.00	0.39058	-	no	1−2 μm	94	46	~15	19
	Crystal	-	-	-	0.39059	no	no	no	87-91	42	7.8+16.5 ~11	7,15−17,20

Conclusions about SrTiO$_3$ ceramics and films:

STO ceramics and polycrystalline films have polar grain boundaries whose effect is revealed both in IR as well as Raman spectra as an appearance of cubic-symmetry forbidden modes (never detected by structural analysis) and in reduced permittivity (compared with crystals) at low temperatures.

(Petzelt et al., PRB **64**, 184111 (2001))

STO epitaxial films ((111) oriented on the (0001) sapphire substrate) display a macroscopic ferroelectric transition probably triggered by the structural order parameter near 120 K with the polarization in the film plane.

Effective dielectric response of polycrystalline STO films is strongly reduced by grain boundaries and particularly by possible nano-cracks.

(Ostapchuk et al., PRB **66**, 235406 (2002))

PbZrO$_3$ (PZ)

First known antiferroelectric with a single 1st order phase transition at 508 K from RT orthorhombic structure Pbam, Z=8, into simple cubic Pm3m , Z=1 phase with a strong C-W type dielectric anomaly. Factor-group analysis (40 atoms in the unit cell, i.e. 120 vibrational degrees of freedom):

16 A$_g$(R) + 12A$_u$ + 16B$_{1g}$(R) + 12B$_{1u}$(IR) + 14B$_{2g}$(R) + 18B$_{2u}$(IR) + 14B$_{3g}$(R) + 18 B$_{3u}$(IR) i.e. 60 Raman and 45 IR modes are expected, which should change to 0 Raman and 3 IR modes in the para-phase.

PbZrO$_3$ crystal

600 K
510 K
473 K
400 K
300 K
10 K

—— IR data
---- fit

Transmitt. at 10 K

Reflect. (trans.)

Wavenumber (cm^{-1})
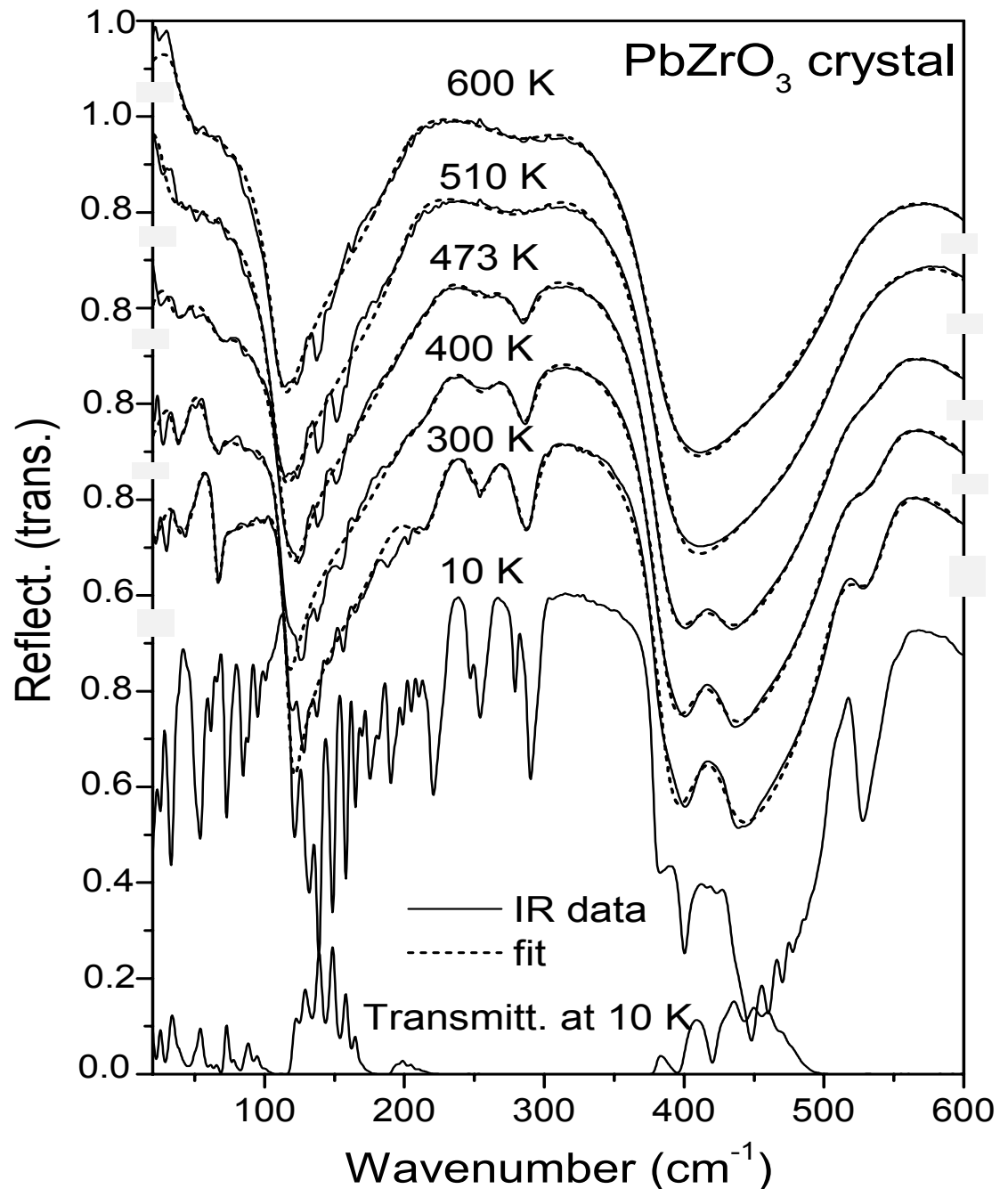
From symmetry point, at least 2 order parameters in the R anf Σ points of the BZ have to be involved, but the ferroelectric Γ-point instability is also very pronounced. IR and MW dielectric data show on a mixed displacive and order-disorder type of the transition – partial softening of a phonon SM and a strong MW central mode

(Ostapchuk et al., J. Phys. CM **13**, 2677 (2001)).
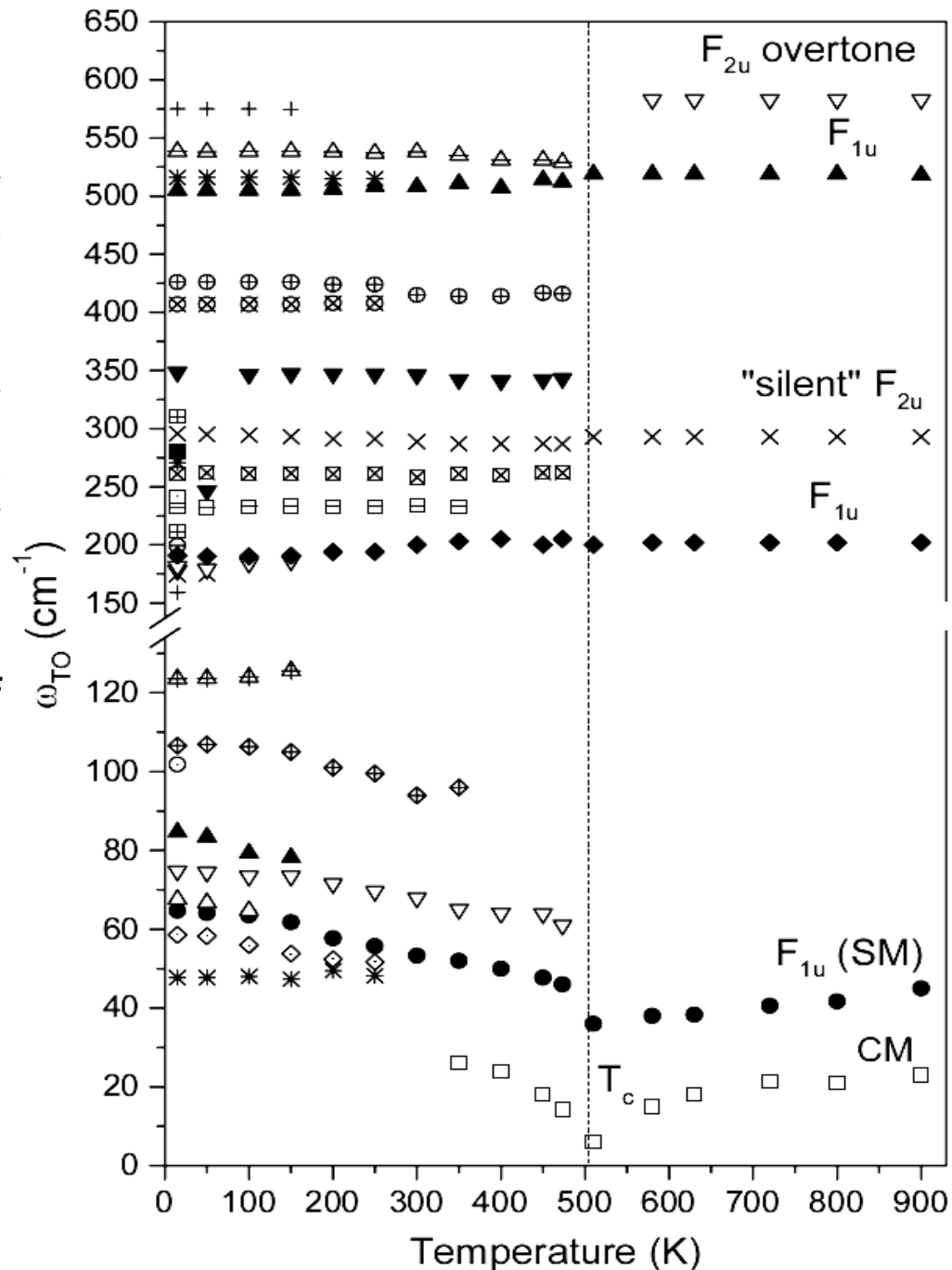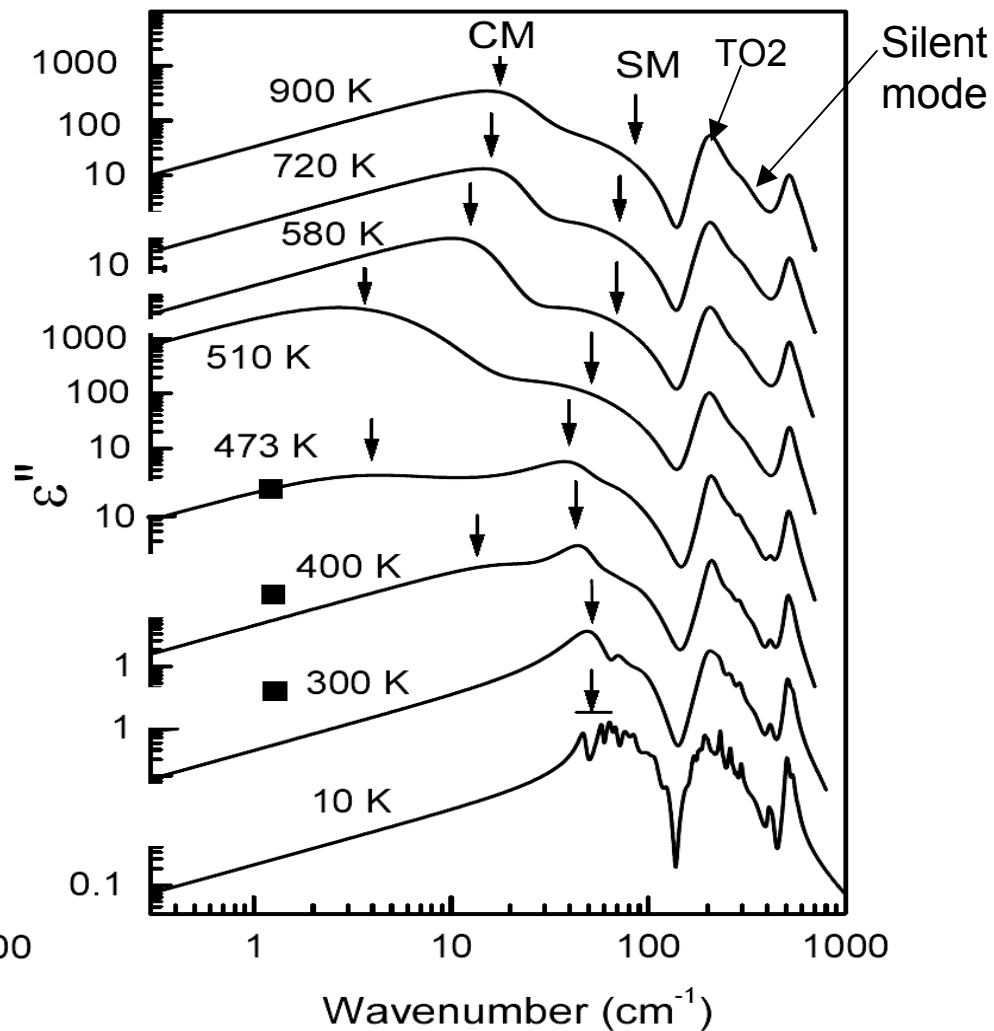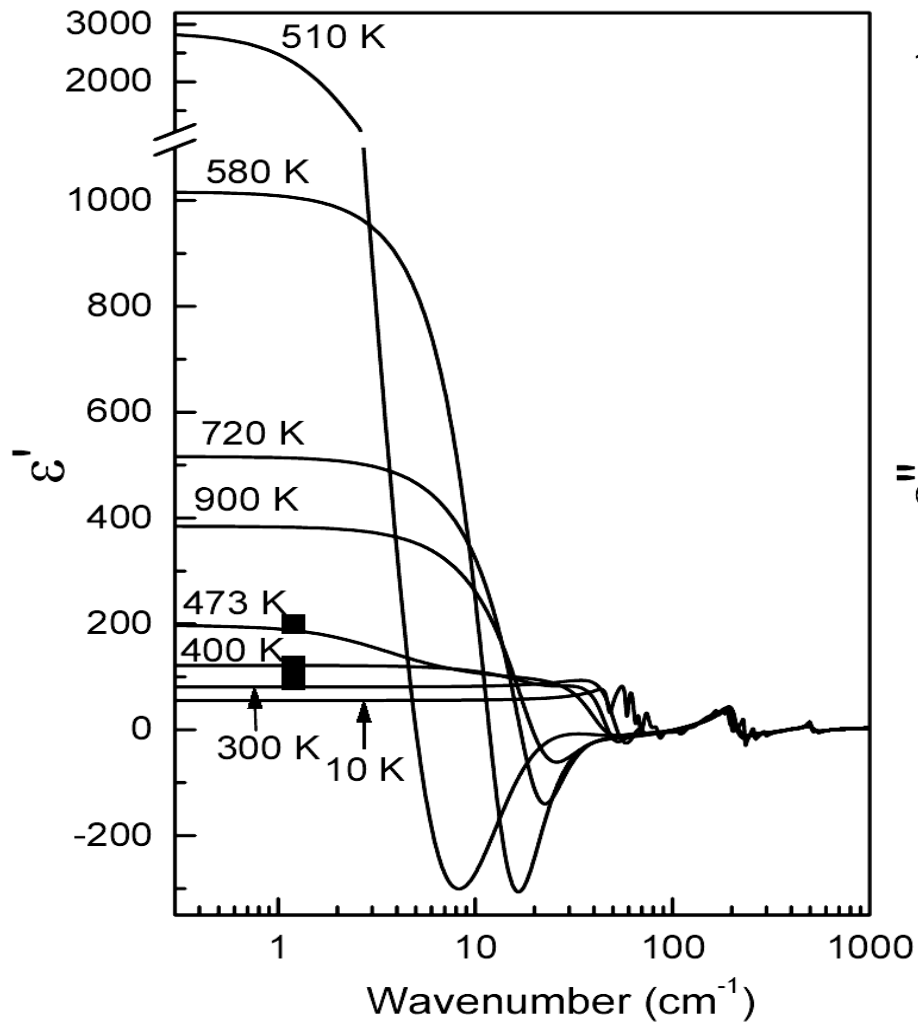
The 4th IR mode at 290 cm^{-1}(forbidden silent F$_{2u}$ mode) and the strong central mode bring evidence for the (probably polar) clusters in the para-phase.

Central mode and phonon contribution to the dielectric response of PbZrO₃
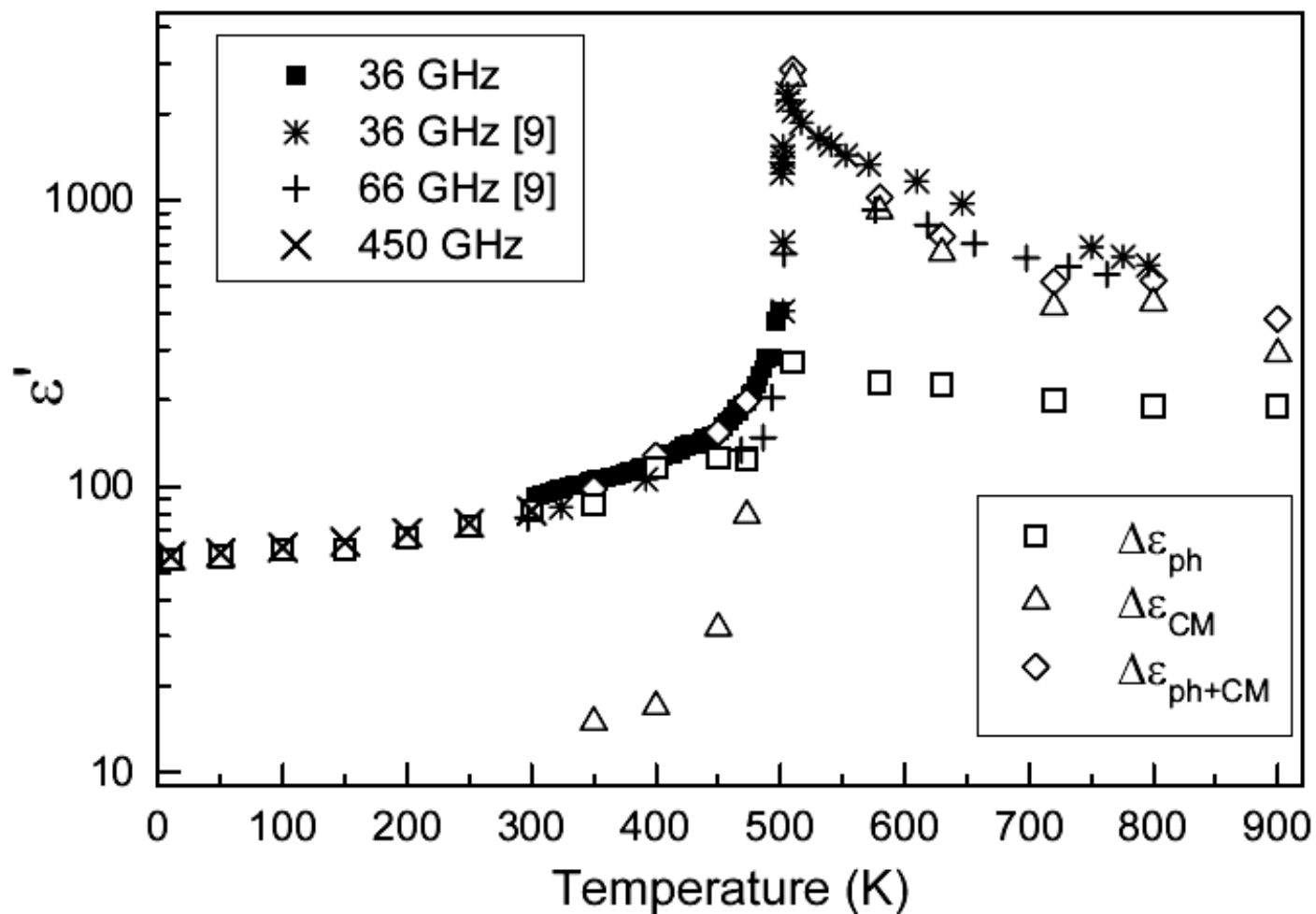
Two dense (98% theor. density) PZ ceramics with different grain structure and completely different dielectric response – effect of nano-cracks

PZ1

PZ2

30 μm

30 μm

$PbZrO_3$, T = 510 K ~ T_c

HF data
on ceramics:
- ☐ PZ1
- △ PZ2
- — CRYSTAL

ε'

PbZrO₃ ceramics
- ■ 1MHz
- ☐ 1GHz

ε'

PZ1

PZ2

Temperature (K)

ε''

CM

SM

BRICK-WALL MODEL
(g=1/3) for
- --- x_1=0.0002
- ⋯ x_2=0.0029

log ν (Hz)
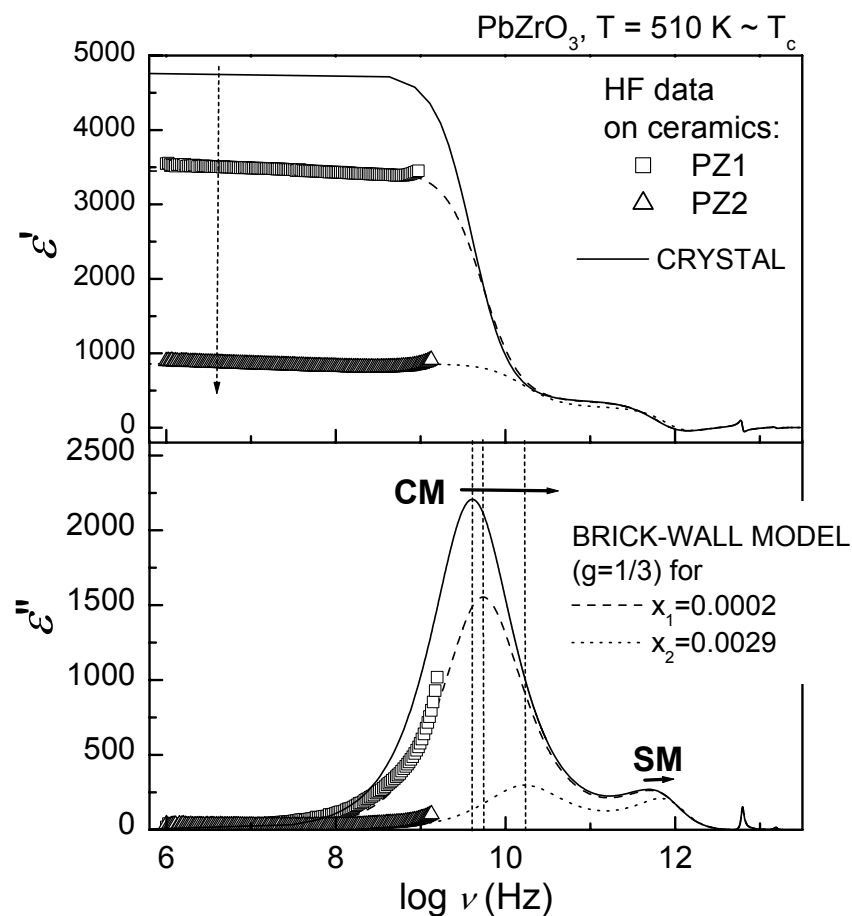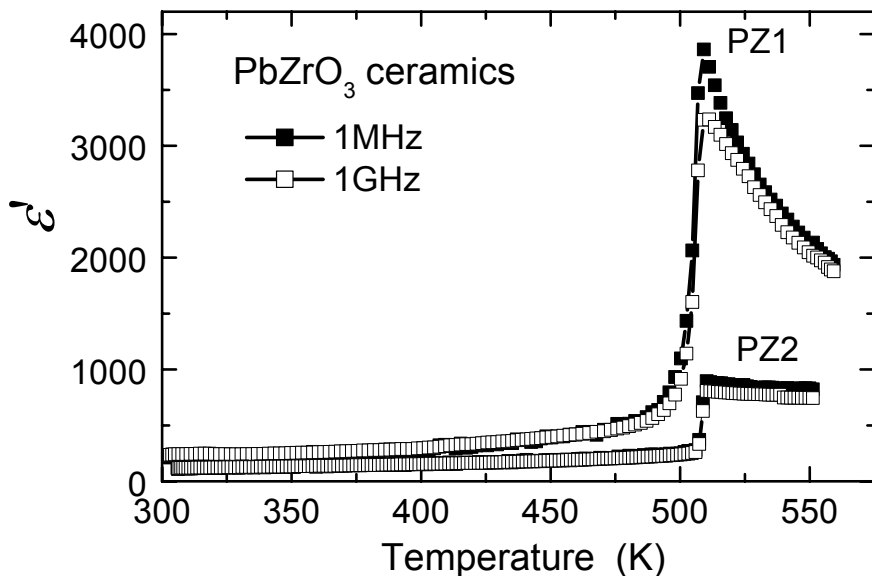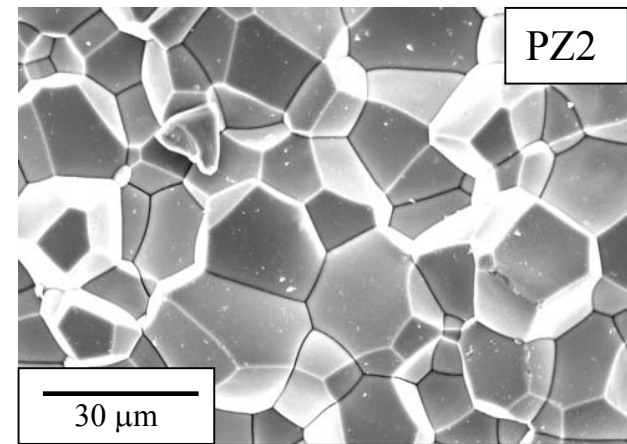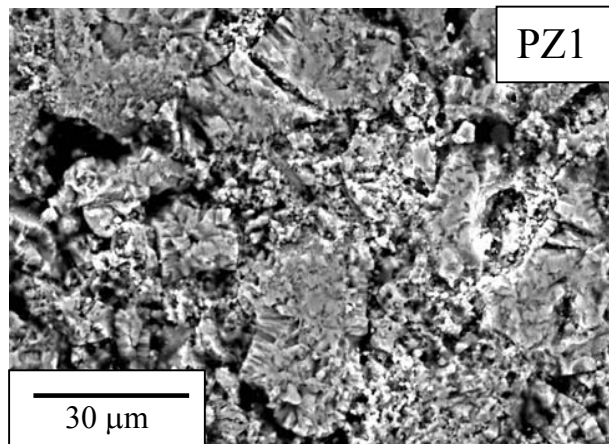
Anisotropic grains: BaTiO$_3$

Phase transitions and factor-group analysis of long-wavelength phonons

Rhombohedral $P_s \parallel (111)$ $C_{3v}^5 (R3_{xyz} m_{\overline{xy}})$			182 K	Orthorhombic $P_s \parallel (110)$ $C_{2v}^{14} (C2_{xy} m_{\overline{xy}} m_z)$			280 K	Tetragonal $P_s \parallel (001)$ $C_{4v}^1 (P4_z m_x m_{xy})$				406 K	Cubic $P_s = 0$ $O_h^1 (Pm\overline{3}m)$			
sp.	activity	ω_0 (?)		sp.	activity	ω_0 (?)		sp.	activity	ω_0	ω_{LO}		sp.	act.	ω_0	ω_{LO}
3A$_1$	IR: E∥P$_s$ R	245-260 180 530		3A$_1$	IR: E∥P$_s$ R	245-265 180 520		3A$_1$	IR: E∥P$_s$ R	230-270 175 510	471 191 725					
				3B$_1$	IR:E∥(011) R	~180 182 490							3F$_{1u}$	IR: TO1 TO2 TO4	10 -170 176 470	175 450 710
3E	IR:E⊥P$_s$ R	~180 182 500		3B$_2$	IR:E∥(101) R	52-62 182 490		3E	IR:E⊥P$_s$ R	35-65 182 470	180 463 717					
1A$_2$	silent	311		1A$_2$	R	311		1B$_1$	R	306						
				1B$_1$	IR:E∥(011) R	311										
1E	IR:E⊥P$_s$ R	311		1B$_2$	IR:E∥(101) R	311		1E	IR:E⊥P$_s$ R	305	306		1F$_{2u}$	TO3 silent	300	
TO: 7(IR+R) LO: 7 R				TO: 12 (IR+R) LO: 12 R				TO: 7(IR+R)+1R LO: 7 R					3 IR			

Order-disorder model for BaTiO$_3$ phase transitions

High Temperature Cubic Phase Paraelectric
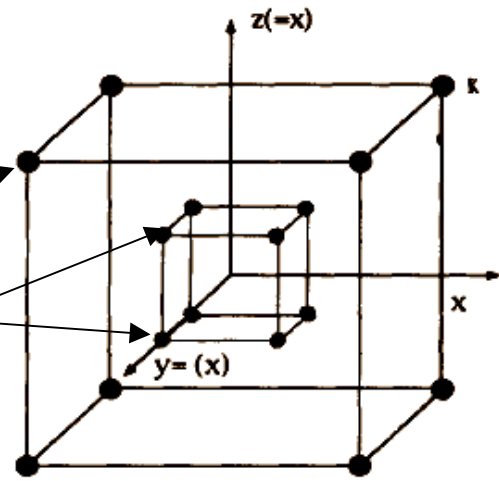
Tetragonal Phase Ferroelectric

Ordered Ba

Dynamically disordered Ti
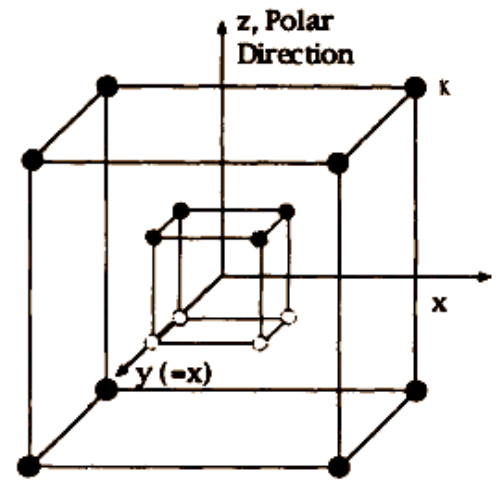
Orthorhombic Phase Ferroelectric
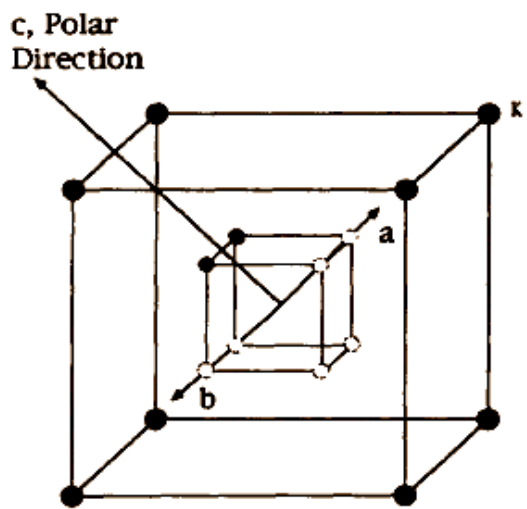
Rhombohedral Phase Ferroelectric
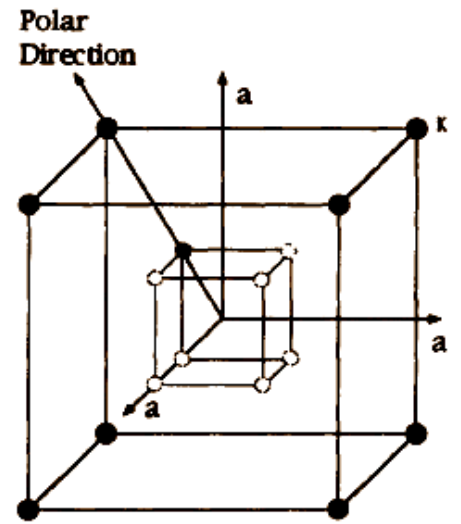
Strong dielectric anisotropy in the tetragonal phase of $BaTiO_3$ single-domain single crystal (from Camlibel et al. J. Phys. Chem. Sol. **31**,1419 (1970)).
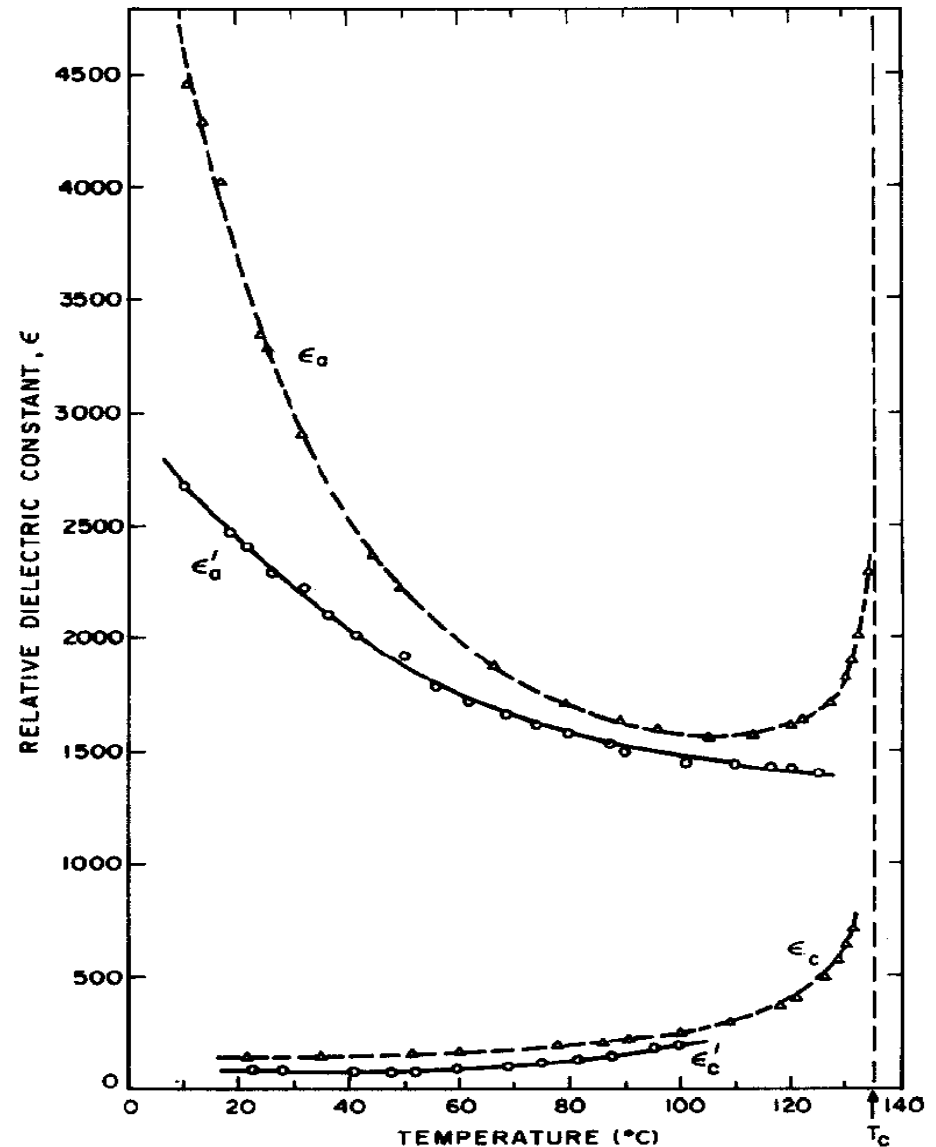
Fig. 1. Temperature dependence of the dielectric constant of melt-grown single-domain $BaTiO_3$ along a and c axes in the tetragonal phase. ϵ_a and ϵ_c refer to the a and c axis unclamped values at $100\,kHz$, and ϵ_c' and ϵ_a' refer to the a and c axis clamped values at $250\,MHz$. The Curie point is $T_c = 133 \pm 2°C$.

Ferroelectric soft-mode behaviour in BaTiO₃ crystals
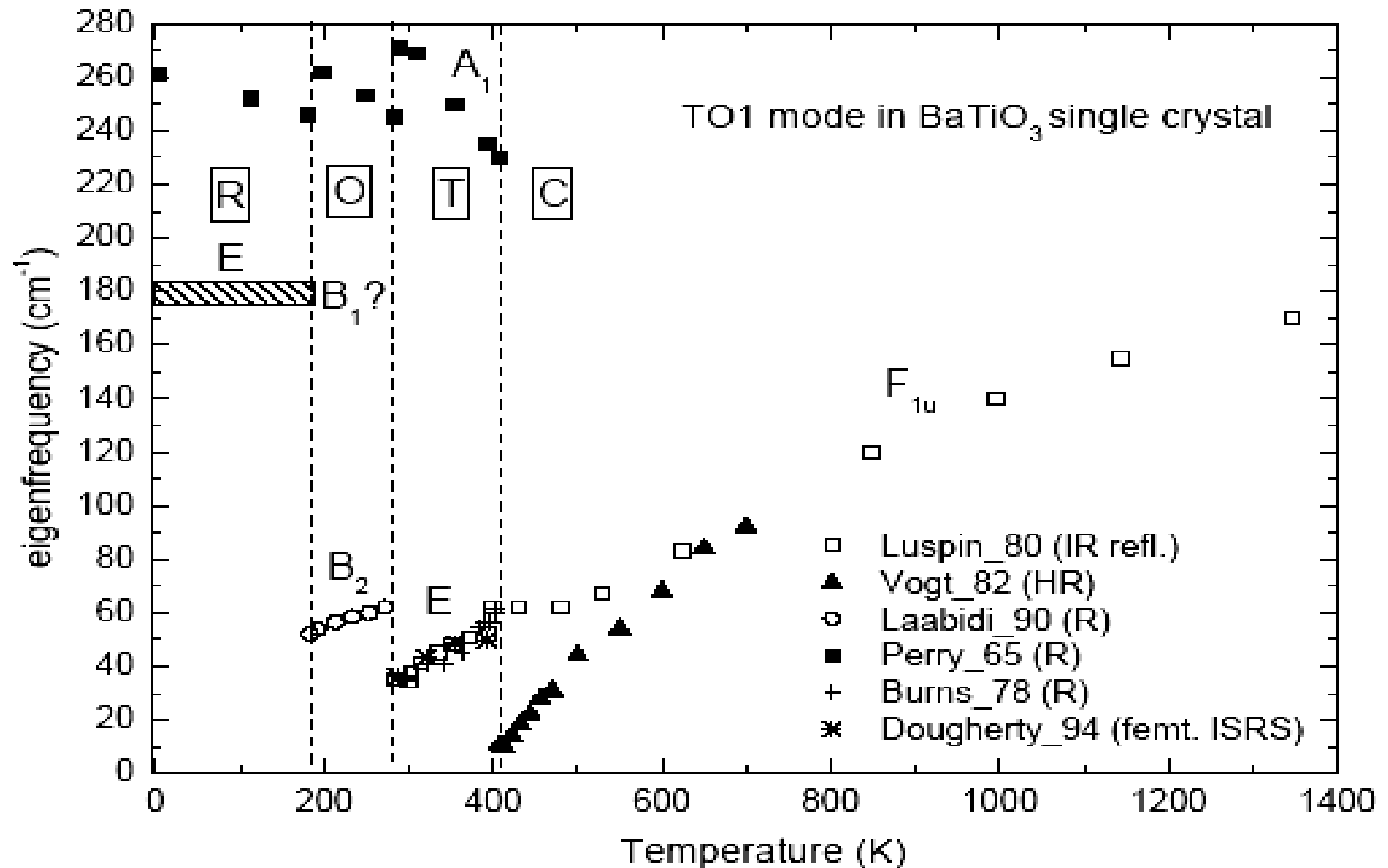
Temperature dependence of the overdamped soft-mode component in BaTiO$_3$.

Plotted is the equivalent Debye-relaxation frequency ω_0^2/γ which corresponds approximately to the maxima in $\varepsilon''(\omega)$ spectra.

BaTiO$_3$ ceramics, 100 nm grains

T=300 K

BWO
TDTS
FTIR
fit

r = 0.3 (plate-like ellipsodal domains (grains))
f = 0.988 (98.8 % density)
f$_C$ = 0.948 (close to Hashin-Shtrickman approximation)

Reflectivity

Wave number (cm^{-1})
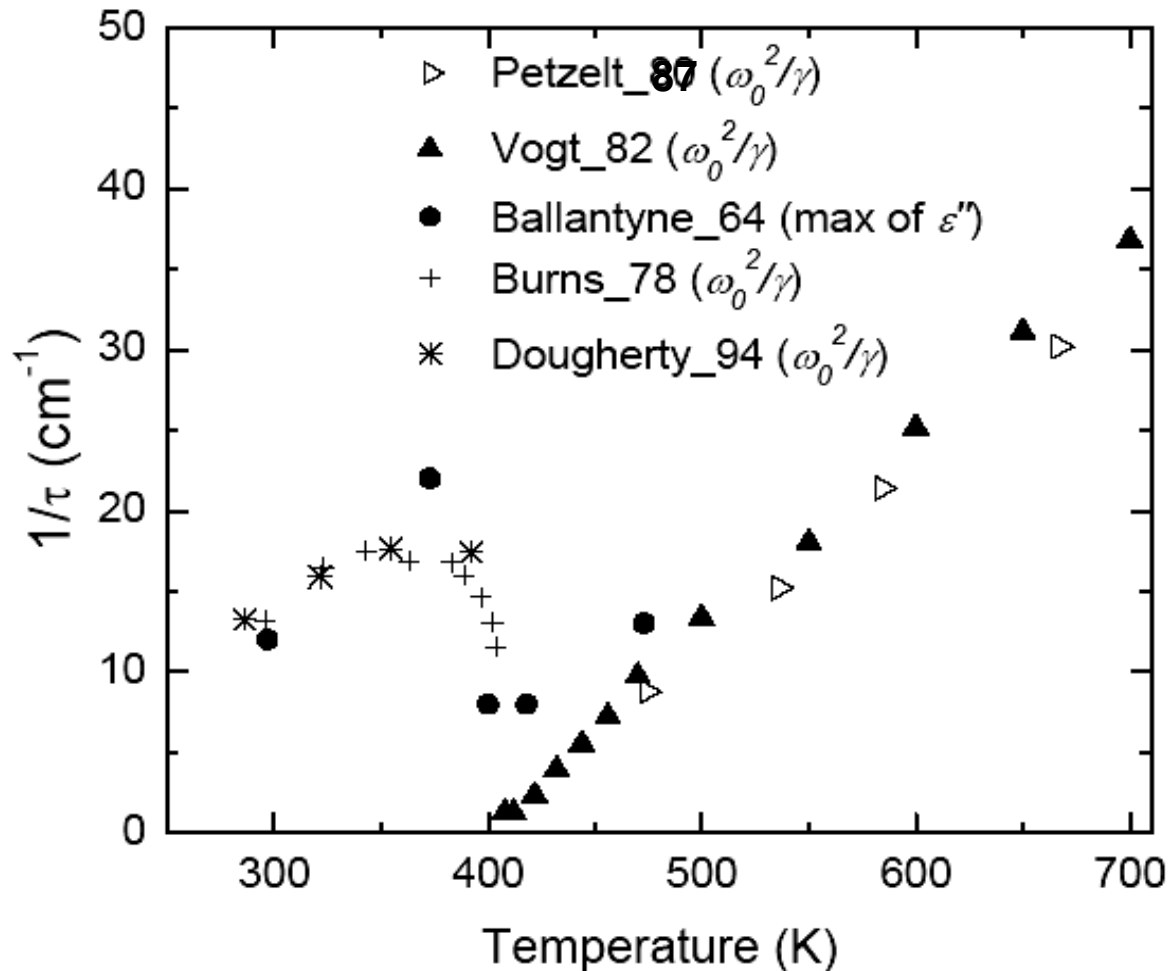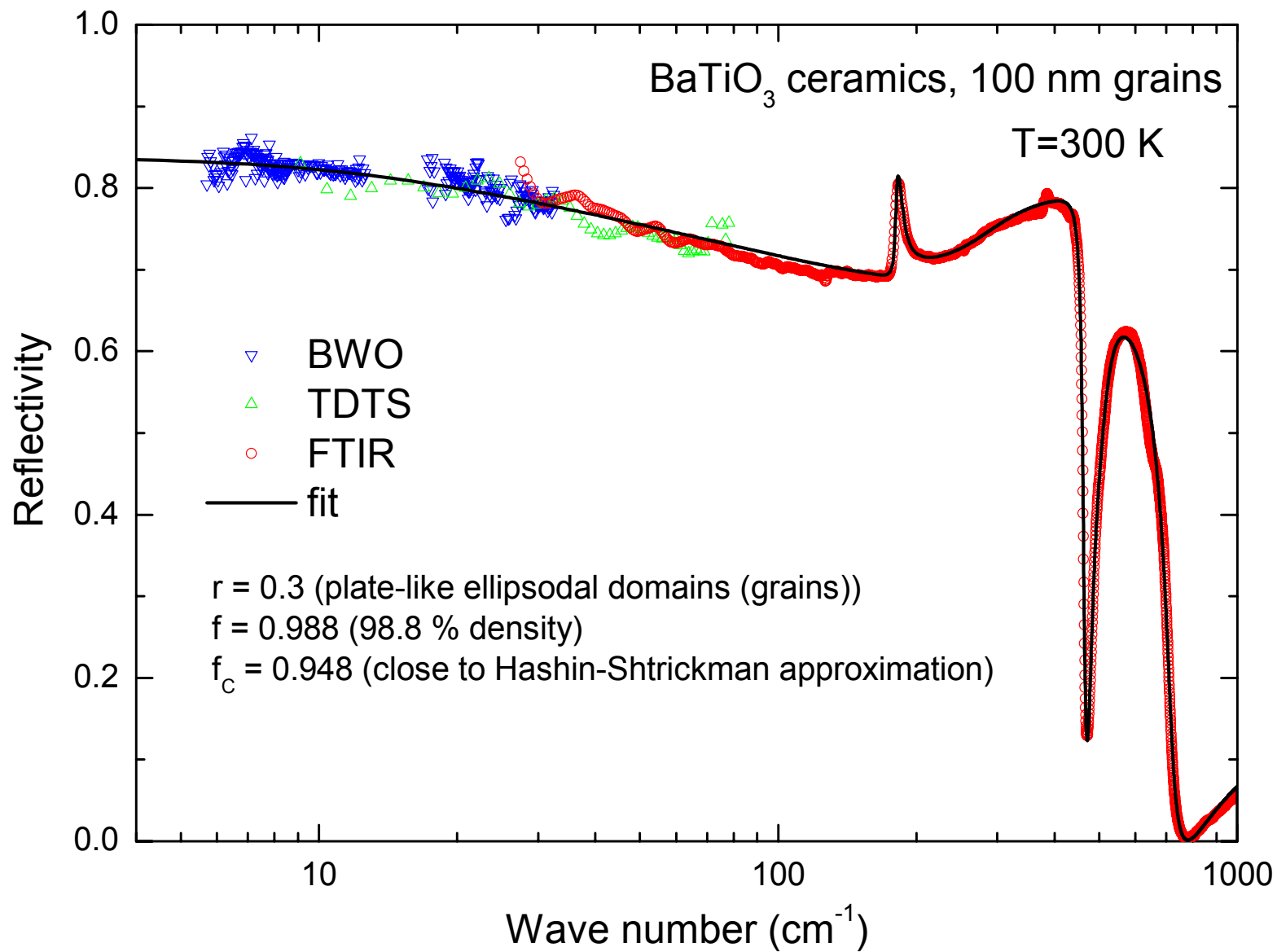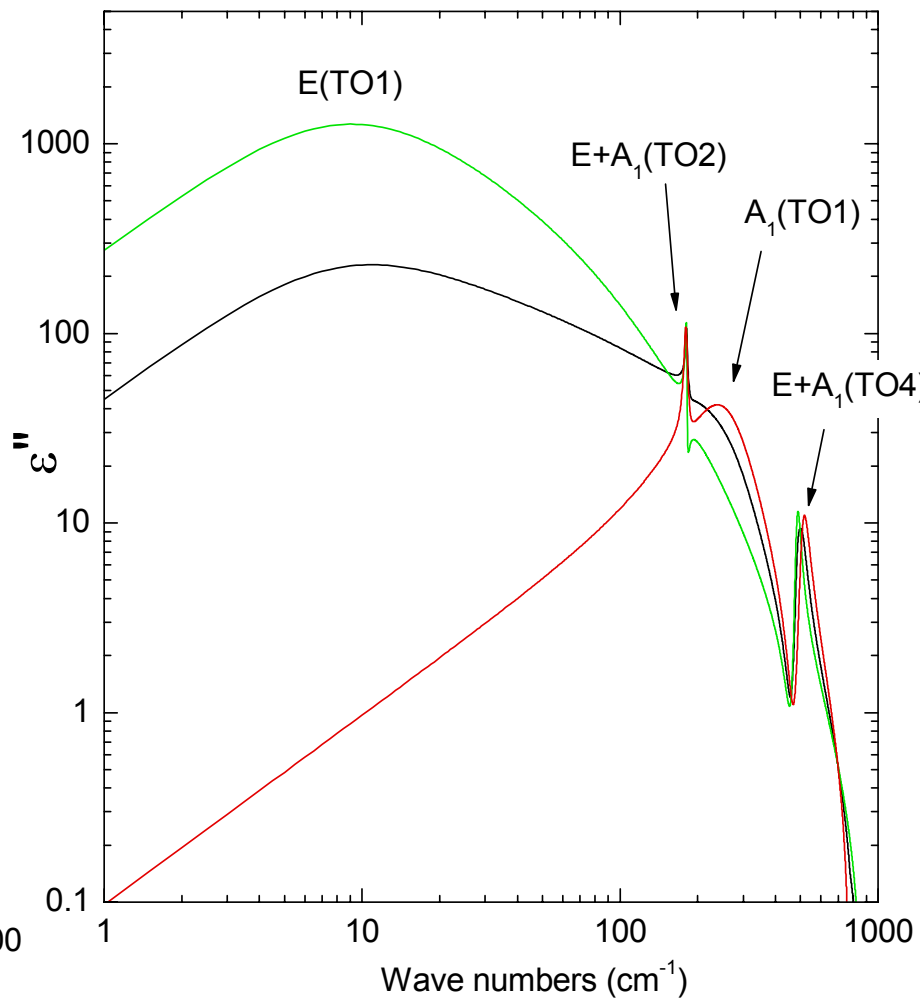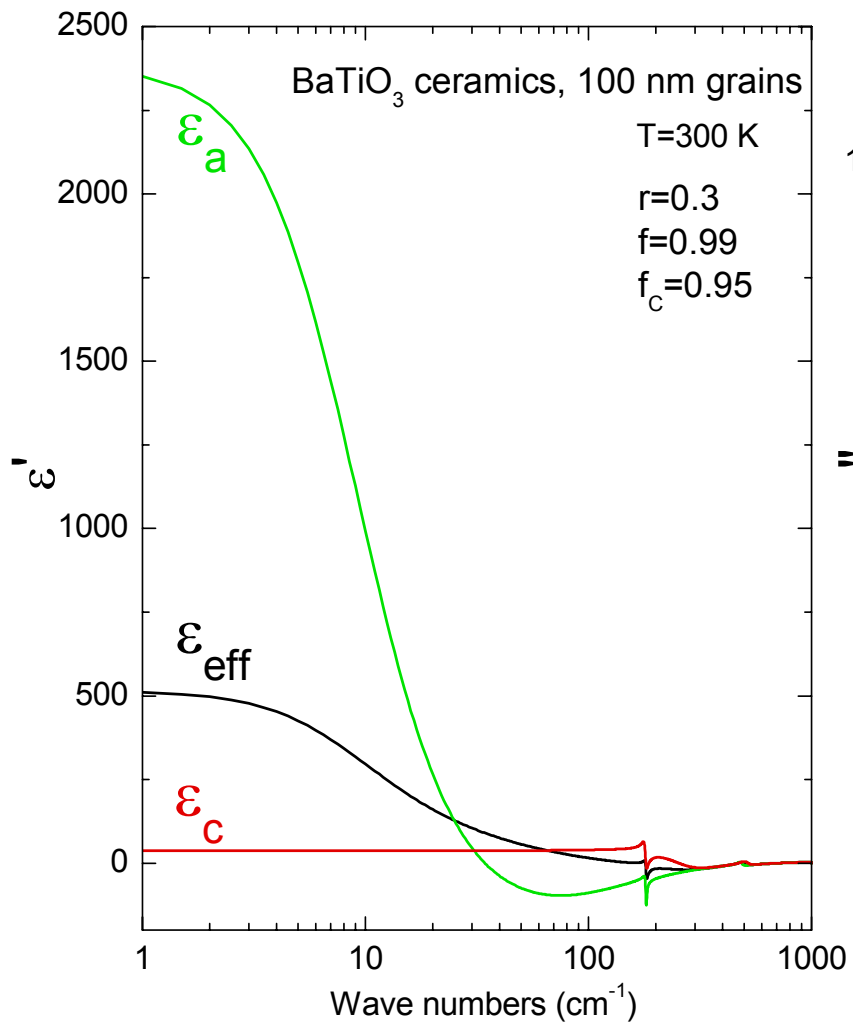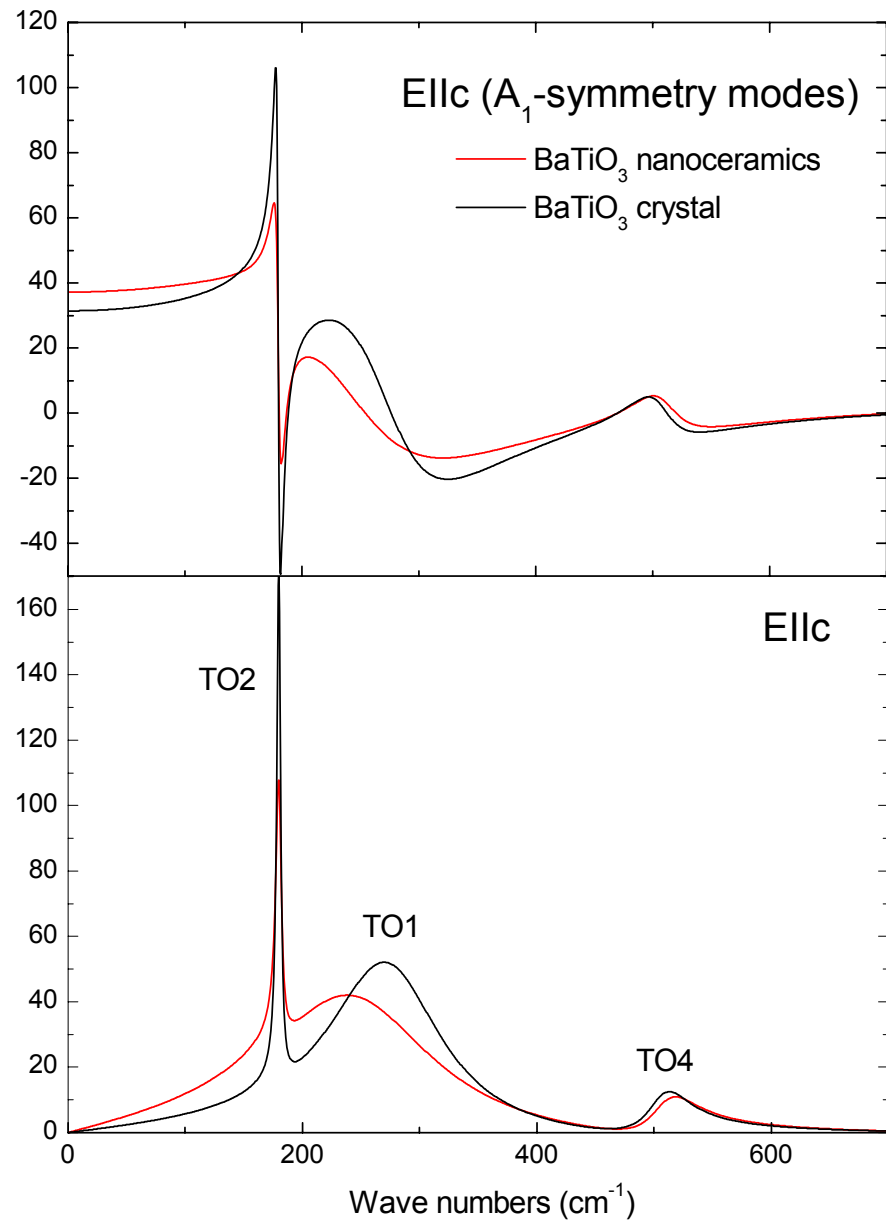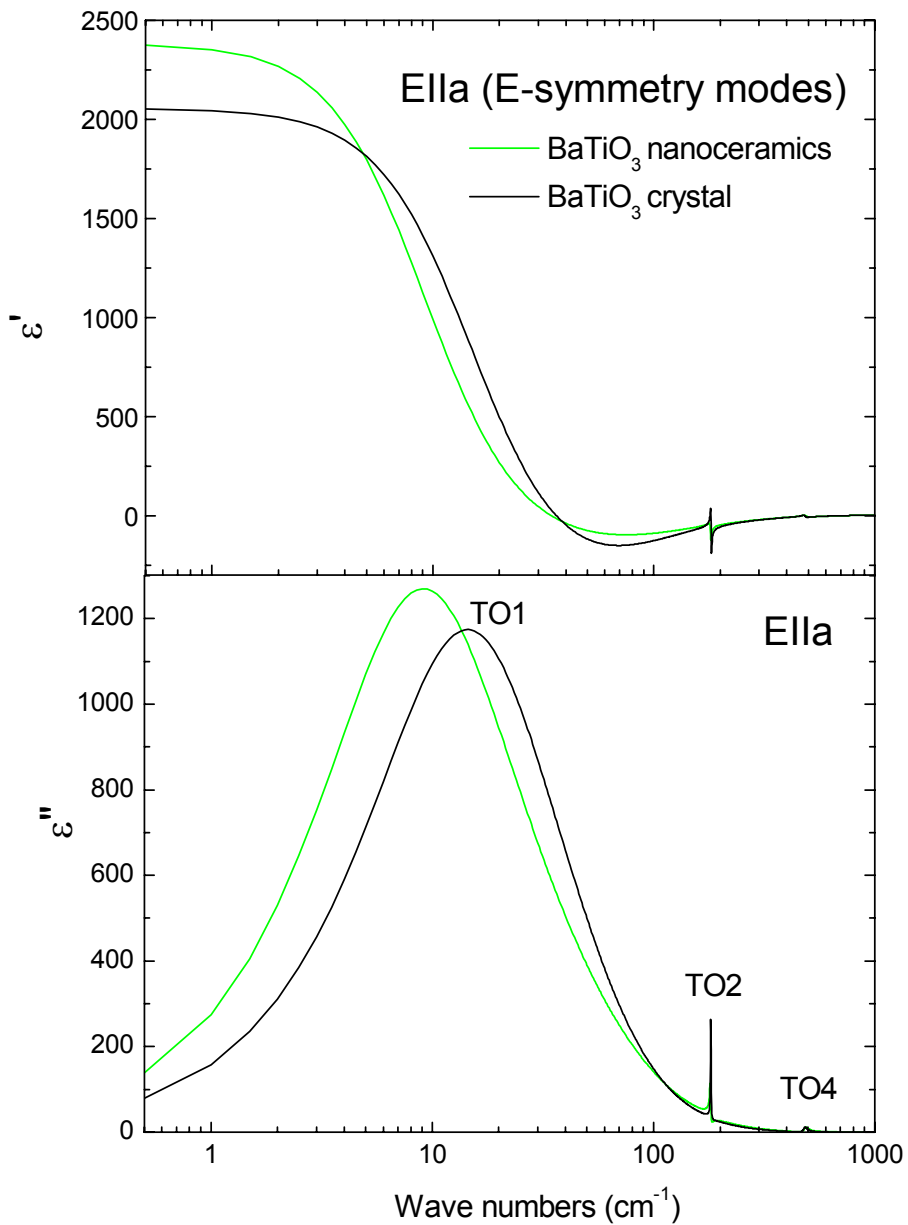
Example of the fitted transmission spectrum of the BTO film + sapphire substrate
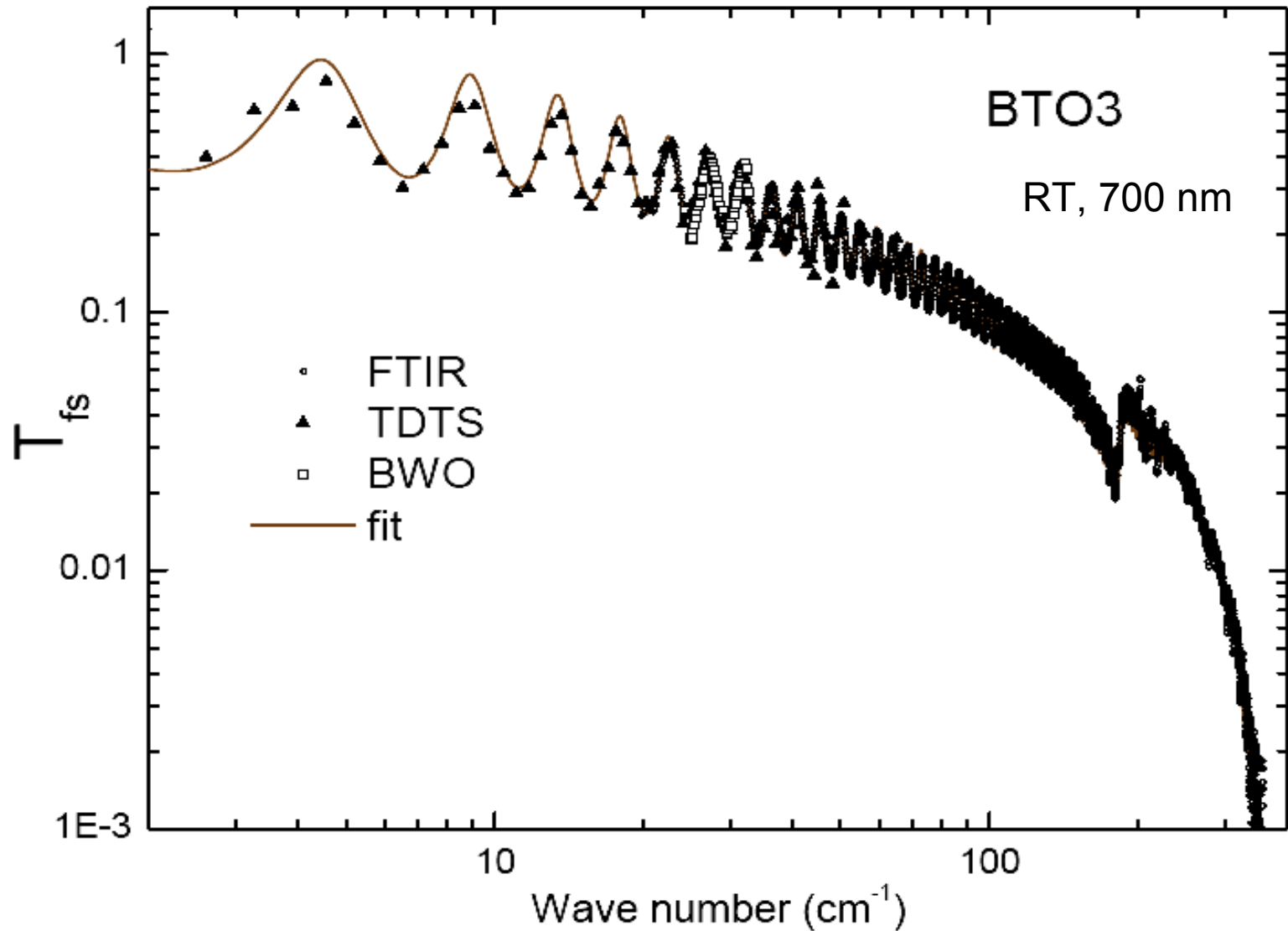
Smoothed relative transmission (with respect to the substrate) and dielectric loss spectra of BTO3 film calculated from the fit to film transmission.
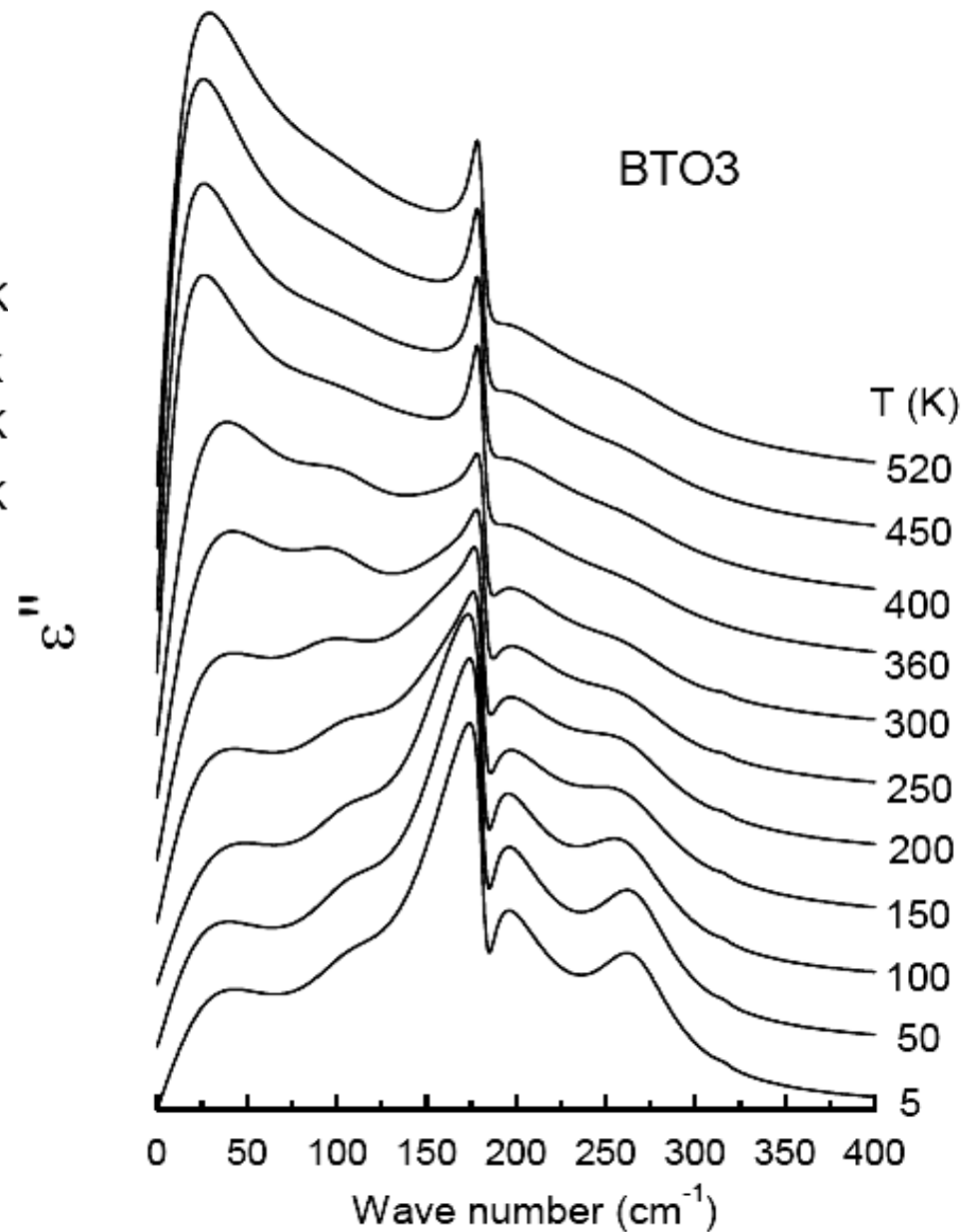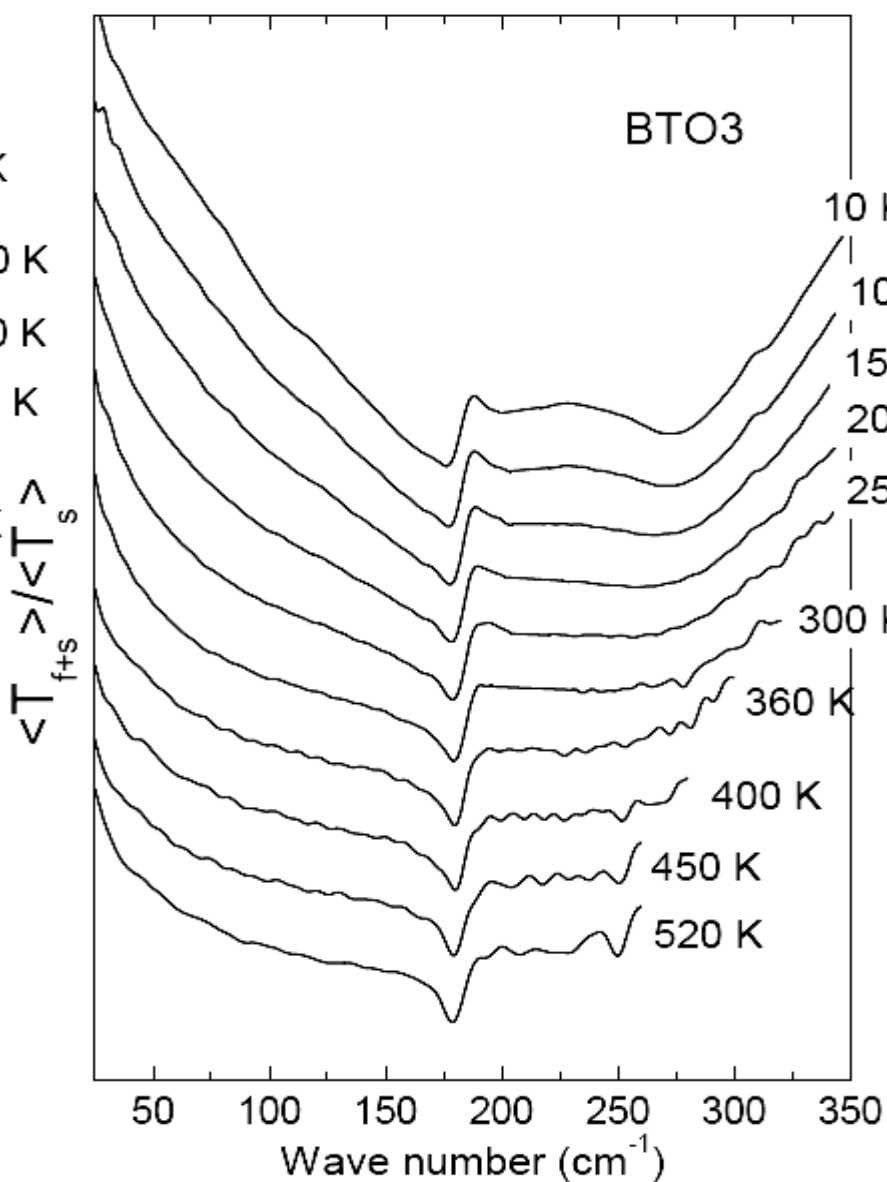
Static permittivity of BTO films from the fit to IR transmission
(polar mode contribution to the permittivity)

Unpolarized Raman spectra of BaTiO₃ crystals (after Perry and Hall 1965)
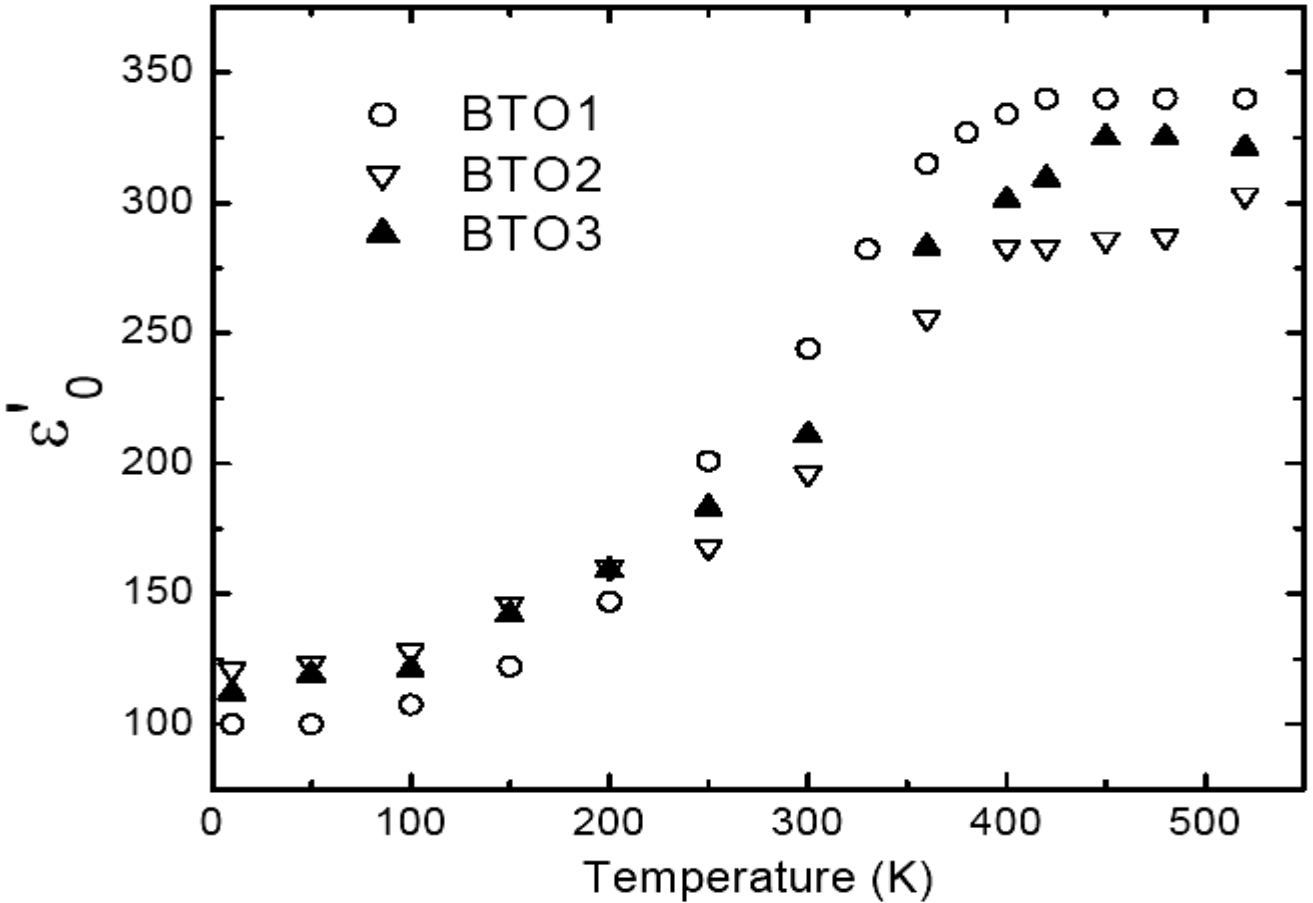
Reduced Raman spectra of a polycrystalline BaTiO₃ film BTO3 and bulk nano-ceramics.
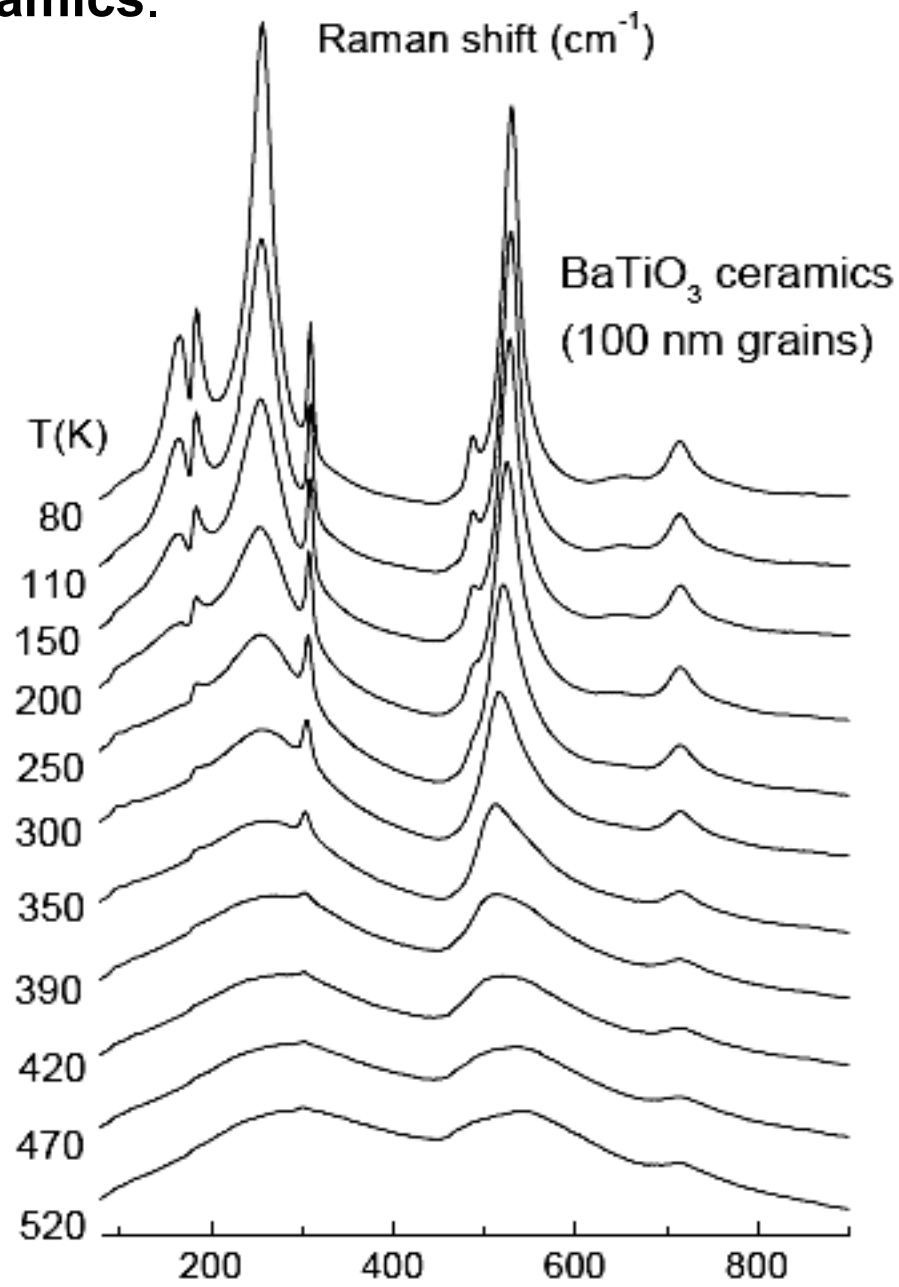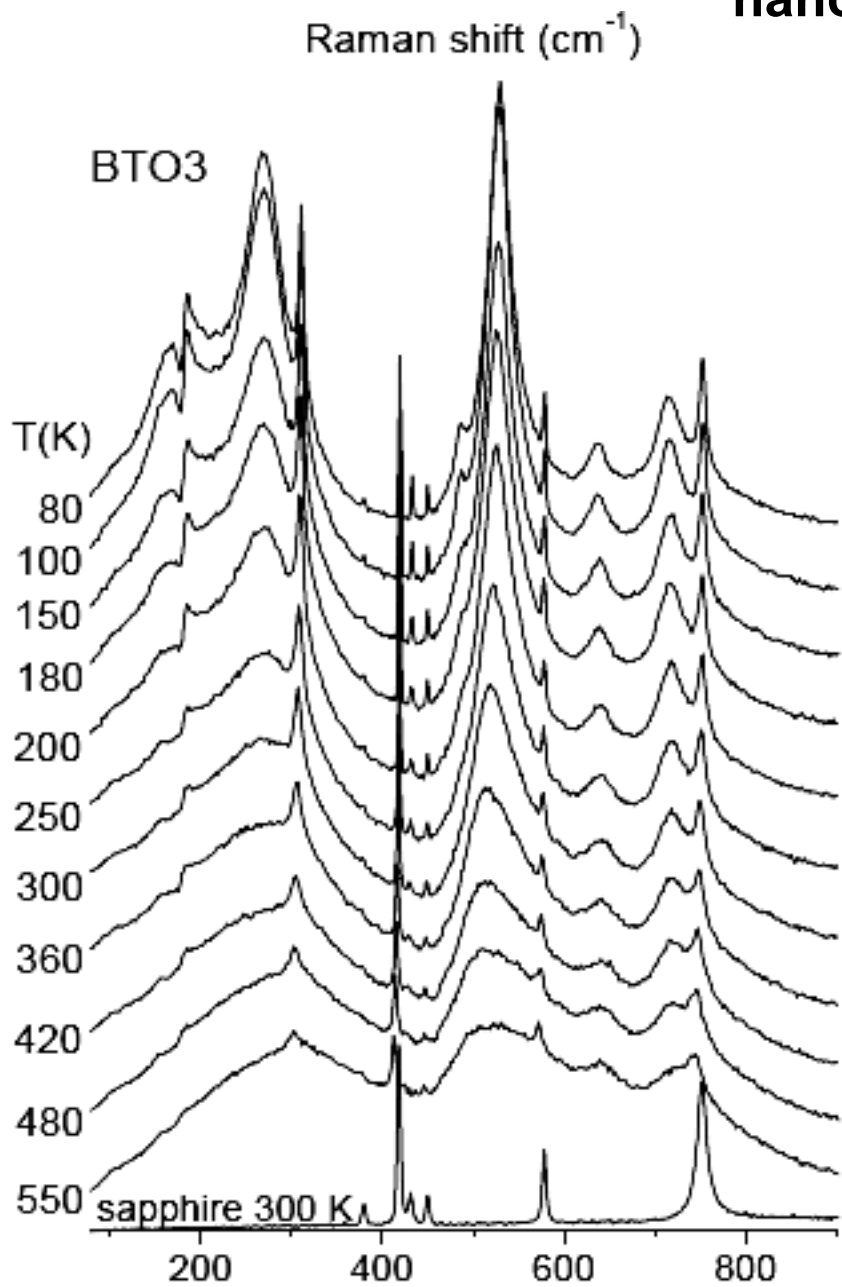
Conclusions

• Dielectric inhomogeneities can substantially influence (mostly reduce) the effective dielectric response, particularly in the case when the high-permittivity component is not percolated. Physically, this is caused by the depolarization field effects on each boundary between different dielectric components.

• The decrease in the static dielectric response has its dynamic counterpart in effective stiffening of the strongest modes in the ac response (soft modes, central modes, critical dielectric relaxations).

• Ceramics can be treated as a special type of composites bulk – grain boundary with non-percolated bulk properties.

• Ceramics with anisotropic grains can be treated as composites with isotropic components of dielectric properties equal to those of principal dielectric responses of anisotropic grains.

• We have not discussed the phenomena connected with non-zero conductivity, which can produce a large variety of non-trivial and pronounced phenomena (like giant permittivity).